ORNL/TM-7512
UC Category Dist. 20d

Contract No. W-7405-eng-26

Engineering Physics Division

Skyshine at Neutron Energies $\leq$ 400 MeV*

R. G. Alsmiller, Jr.
J. Barish+
R. L. Childs+

DISCLAIMER

This book was prepared as an account of work sponsored by an agency of the United States Government. Neither the United States Government nor any agency thereof, nor any of their employees, makes any warranty, express or implied, or assumes any legal liability or responsibility for the accuracy, completeness, or usefulness of any information, apparatus, product, or process disclosed, or represents that its use would not infringe privately owned rights. Reference herein to any specific commercial product, process, or service by trade name, trademark, manufacturer, or otherwise, does not necessarily constitute or imply its endorsement, recommendation, or favoring by the United States Government or any agency thereof. The views and opinions of authors expressed herein do not necessarily state or reflect those of the United States Government or any agency thereof.

*Submitted for Journal publication

+Computer Sciences Division

Date Published - October 1980

NOTICE This document contains information of a preliminary nature. It is subject to revision or correction and therefore does not represent a final report.

OAK RIDGE NATIONAL LABORATORY
Oak Ridge, Tennessee 37830
operated by
UNION CARBIDE CORPORATION
for the
U. S. DEPARTMENT OF ENERGY

This document is
PUBLICLY RELEASABLE
Larry E. Williams
Authorizing Official
Date: 01/31/2006

DISTRIBUTION OF THIS DOCUMENT IS UNLIMITED

DISCLAIMER

This report was prepared as an account of work sponsored by an agency of the United States Government. Neither the United States Government nor any agency Thereof, nor any of their employees, makes any warranty, express or implied, or assumes any legal liability or responsibility for the accuracy, completeness, or usefulness of any information, apparatus, product, or process disclosed, or represents that its use would not infringe privately owned rights. Reference herein to any specific commercial product, process, or service by trade name, trademark, manufacturer, or otherwise does not necessarily constitute or imply its endorsement, recommendation, or favoring by the United States Government or any agency thereof. The views and opinions of authors expressed herein do not necessarily state or reflect those of the United States Government or any agency thereof.

DISCLAIMER

Portions of this document may be illegible in electronic image products. Images are produced from the best available original document.

ACKNOWLEDGMENT

Thanks are extended to Dr. P. Gollon of the ISABELLE staff at the Brookhaven National Laboratory for many helpful discussions throughout the course of this work.

TABLE OF CONTENTS

Chapter	Page
ABSTRACT	vii
1 INTRODUCTION	1
2 IMPORTANCE FUNCTIONS	2
3 COMPARISONS WITH EXPERIMENTAL DATA	13
4 CALCULATIONS TO DETERMINE THE ROOF THICKNESS OVER A TARGET AREA FOR A 400 GEV PROTON ACCELERATOR	16
4.1 Neutron Source	16
4.2 Dose Equivalent vs. Radial Distance from the Source for Various Roof Thicknesses	22
APPENDIX A	27
APPENDIX B	33

ABSTRACT

The dose equivalent at an air-ground interface as a function of distance from an assumed azimuthally symmetric point source of neutrons can be calculated as a double integral. The integration is over the source strength as a function of energy and polar angle weighted by an importance function that depends on the source variables and on the distance from the source to the field point. The neutron importance function for a source 15 m above the ground emitting only into the upper hemisphere has been calculated using the two-dimensional discrete ordinates code, DOT, and the first collision source code, GRTUNCL, in the adjoint mode. This importance function is presented for neutron energies $\leq$ 400 MeV, for source cosine intervals of 1 to .8, .8 to .6, .6 to .4, .4 to .2 and .2 to 0, and for various distances from the source to the field point. As part of the adjoint calculations a photon importance function is also obtained. This importance function for photon energies $\leq$ 14 MeV and for various source cosine intervals and source-to-field point distances is also presented. These importance functions may be used to obtain skyshine dose equivalent estimates for any known source energy-angle distribution.

To illustrate the use of the results, the dose equivalent as a function of distance from one of the target areas at the Alternating Gradient Synchrotron at the Brookhaven National

Laboratory has been calculated and is compared with the experimental data of C. Distenfeld and D. Colvett. The energy-angle distribution of the neutron source used in this calculation was taken from the measurements of R. Madey, A. R. Baldwin and F. W. Waterman.

To aid in the design of the roof over a target area for the 400 GeV proton accelerator, ISABELLE, being constructed at the Brookhaven National Laboratory, the dose equivalent as a function of distance from the target area and as a function of roof thickness has been calculated and is presented. The energy-angle distribution of the neutrons emerging from the roof over the target area was calculated as a function of roof thickness using the high-energy transport code, HETC. The dose equivalent from these neutrons has been calculated using the importance results. Also, in one case, the dose equivalent has been calculated directly with the discrete ordinates codes and a comparison between dose equivalent as a function of distance obtained by direct calculation and using adjoint methods is given.

1 INTRODUCTION

In designing the shielding for high-energy accelerators it is necessary to consider the radiation that passes into the atmosphere from the top of the shield and is scattered back to the earth producing a radiation field at distances reasonably removed (∿1000 m) from the accelerator. This phenomena is usually called "skyshine" and has been studied by a variety of investigators.[1-3] In this paper two-dimensional discrete ordinates methods are used to obtain, numerically, importance functions that may be used to estimate the dose equivalent from skyshine. The importance functions are given for a neutron (and/or photon) source 15 m above the ground and emitting only into the upper hemisphere. These functions are presented for neutron energies $\leq$ 400 MeV, for photon energies $\leq$ 14 MeV, for various source cosine intervals, and for various source-to-field point distances. The upper limit on the neutron energy is dictated by practical consideration, i.e., it is below the effective pion production threshold, but it is sufficiently large for most applications even around very high-energy accelerators.[1-3]

To illustrate the use of the neutron importance functions, and to demonstrate the accuracy that can be obtained, calculations have been carried out and compared with experimental data taken by C. Distenfeld and D. Colvett.[2] Also a series of calculations have been carried out to aid in the design of the shielding for the 400 GeV storage ring, ISABELLE,[4] under construction at the Brookhaven National Laboratory.

In Section 2 the importance function calculations are described and the neutron importance function is presented and discussed. The photon importance function is given in Appendix A. In Section 3 calculated results for the dose equivalent as a function of distance from one of the target areas at the Alternating Gradient Synchrotron at the Brookhaven National Laboratory are presented and compared with experimental data. In Section 4 calculated results for the skyshine dose equivalent from a 400 GeV accelerator target area are presented and discussed. A signficant part of this calculation is the method used to determine the neutron source as a function of roof thickness and the details of these calculations are also presented in Section 4.

2 IMPORTANCE FUNCTIONS

Before describing the calculations of the importance functions, the manner in which they are to be used will be incidated. The dose equivalent, $D_i(\overline{r})$ due to source particles may be written

$$D_i(\overline{r}) = \int S_i(E,\cos\Theta) I_i(E,\cos\Theta,\overline{r}) dEd \qquad (1)$$

where

i = n for neutrons and γ for protons,

$S_i(E,\cos\Theta)$ = the number of source particles of type i per unit solid angle at energy E and polar angle Θ (the source is by assumption independent of the azimuthal angle),

$I_i(E,\cos\Theta,\bar{r})$ = the importance of particles of type i at energy E and polar angle Θ and average radial distance $\bar{r}$.

It is to be understood that Eq. (1) is for the dose equivalent at the air-ground interface. If the source contains both neutrons and photons, the total dose equivalent is the sum of the dose equivalents for the two values of i. For many applications the dose equivalent contribution from source photons is small compared to the contribution from source neutrons and thus the importance function for photons is not nearly as significant as that for neutrons. For this reason, and because the photon importance function is not used in Section 3 and 4 of this paper, it will not be presented in this section, but it is given in Appendix A. It is, perhaps worth noting that the dose equivalent given by Eq. (1) for i = n does contain the contribution to the dose equvialent at $\bar{r}$ due to photons that are produced by neutron-nucleus collison and reach the detector.

A schematic diagram of the geometry (cylindrical) for which the importance functions have been calculated is shown in Fig. 1. The point source is 15 m above the air-ground inter-

ORNL-DWG 80-15603

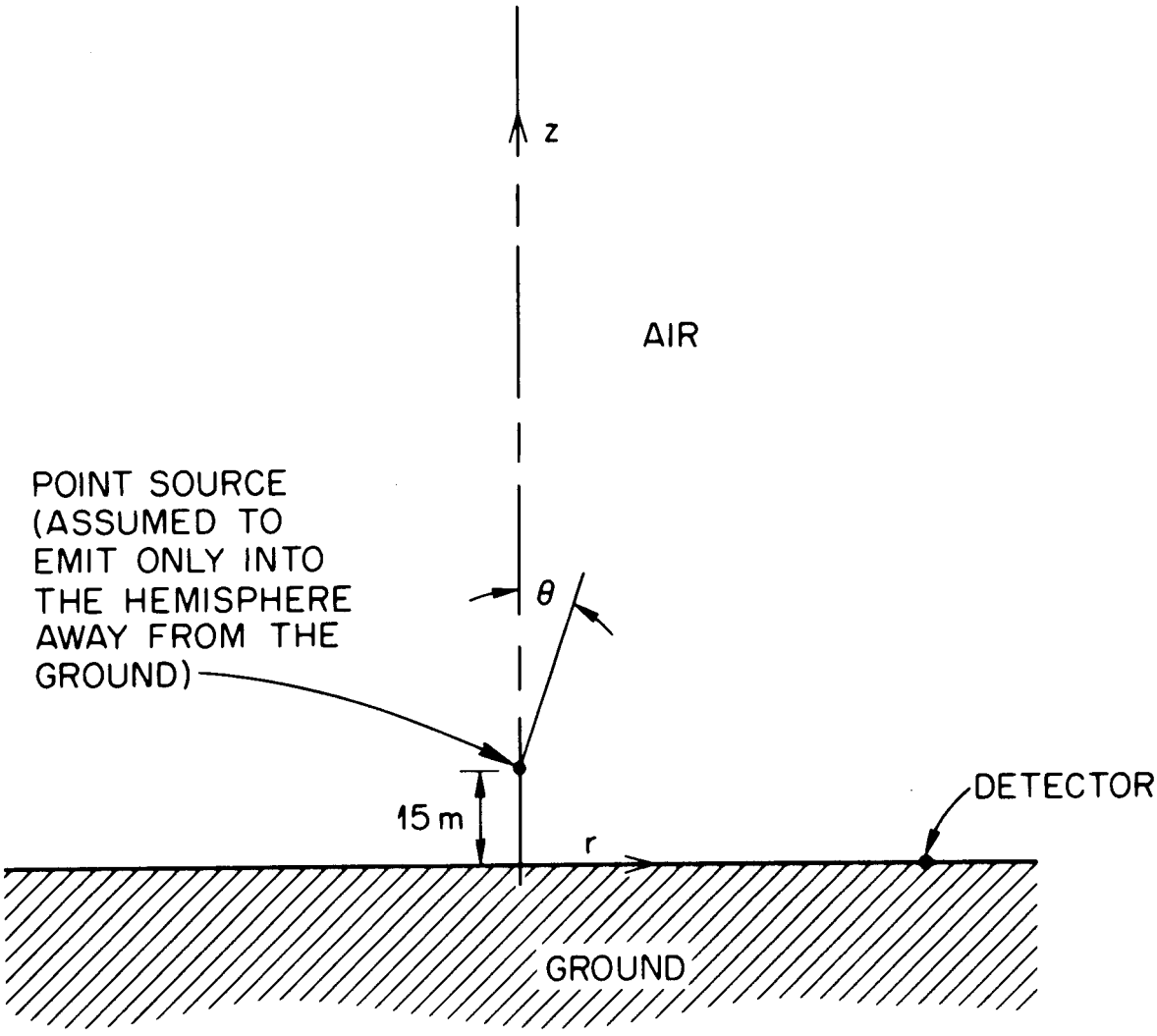

Fig. 1. Schematic diagram of geometry for which importance functions are calculated.

face and is assumed to emit only into the hemisphere away from the ground. Cylindrical symmetry about the z axis is assumed. The point source may emit neutrons, photons, or a combination thereof.

Air was assumed to be composed of 79% nitrogen and 21% oxygen and to have a density of 1.20×10^{-3} g/cm^3. Ground was assumed to be silicon dioxide with 5% water by weight and to have a density of 1.8 g/cm^3.

At neutron energies $\leq$ 60 MeV the multigroup cross section data for hydrogen, oxygen, and silicon were taken from Ref. 5. Multigroup cross section data for nitrogen at energies $\leq$ 60 MeV were prepared using the same methods and codes as those used in Ref. 5. Above 60 MeV differential cross section data for neutron-nucleus nonelastic collisions were taken from Refs. 6 and 7 and differential cross section data for elastic collisions were obtained using the optical model code GENOA* and the parameters of F. D. Bercchette and G. W. Greenless.[8] It should be noted that photon production from neutron-nucleus collisions at energies $\geq$ 15 MeV are not available, and in all of the calculations reported in this paper it is assumed that this photon production may be neglected.[9] Photon multigroup cross sections were taken from Ref. 10.

---

*This is an undocumented optical model code written by F. G. Perey at the Oak Ridge National Laboratory.

The neutron flux-to-dose equivalent rate conversion factors were taken from the recommendation of the National Council on Radiation Protection[11] and the photon flux-to-dose equivalent ratio conversion factors were taken from the work of H. C. Claiborne and D. K. Trubey.[12]

All of the calculations were carried out with the two-dimensional discrete ordinates code, DOT,[13] and the first collision source code, GRTUNCL*, all in the adjoint mode. The first collision source code is used to avoid ray effects in the discrete ordinates calculations.

It was determined numerically that the results were essentially unchanged if the top of the atmosphere was taken to be 555 m, if the ground thickness was taken to be 0.5 m, and if the radial boundary was taken to 1560 m, so these values were used. Since for the highest energy considered here the mean free path for a nonelastic collision in the atmosphere is of the order of 770 m, the height of the atmosphere is taken to be somewhat less than a mean free path. The fact that this assumed height is adequate for the calculations considered here is very dependent on the energy-angle correlation of neutrons produced from medium energy neutron-nucleus collisions, i.e., only low energy neutrons are produced at large backward angles, and on the fact that only detector locations in the vicinity of the air-ground inter-

*This is an undocumented code written by R. L. Childs at the Oak Ridge National Laboratory. A brief description of the theory of the code will be found in Ref. 14.

face are considered. The calculations were carried out using 37 axial mesh intervals in the air, 14 axial mesh intervals in the ground, and 62 radial mesh intervals. The angular dependence of the cross sections for all nuclei was approximated using a P_3 Legendre expansion corrected to a P_2 Legendre expansion assuming a delta function in the forward direction.[15,16] The delta function correction is used here to account for the fact that elastic scattering becomes very forward at the higher energies considered here. All of the calculations were carried out using a S_8 angular quadrature.

Neutron and photon importance has been calculated for all neutron energies $\leq$ 400 MeV, for all photon energies $\leq$ 14 MeV, for source cosine intervals of 1 to .8, .8 to .6, .6 to .4, .4 to .2, and .2 to 0, and for average radial distances (with the source at radius 0.0) of 11, 108, 495, and 1005 m, and at the air-ground interface. These radial distances are the midpoint of the mesh intervals used. Because of the finite difference procedure used, the adjoint results correspond to averages over the detector radial intervals 9 to 13 m, 96 to 120 m, 480 to 510 m, and 990 to 1020 m, respectively. Also, because of the finite difference procedure used, the values given for the air-ground interface correspond to an average over an interval of 1 m (in air)

immediately adjacent to the actual air-ground interface. The fact that the source is 15 m above the air-ground interface does enter into the calculations. Strictly speaking, the results are not applicable to other vertical source locations, but to a reasonable approximation they may be applied to other locations that are not markedly different from those used here.

In Figs. 2 through 5 the neutron importance is shown as a function of energy for specified cosΘ intervals.* Each figure corresponds to a different value of $\bar{r}$ as indicated. The histogram interval used in the figures corresponds to the energy group structure used in the calculation. In a given figure the curves for the different cosine intervals are very similar, but there are numerical differences. The structure in the curve below approximately 15 to 20 MeV is due to resonances in the cross sections. By comparing the corresponding curve in the various figures it is clear that the relative importance of high energy neutrons changes substantially with $\bar{r}$. That is, at $\bar{r}$ = 1005 m (Fig. 5) the highest energy neutrons considered are much more important than neutrons in the 1 MeV energy range, while at $\bar{r}$ = 11 m (Fig. 2) the most importance is associated with neutrons in the few MeV range and the very high energy neutron has a relatively small importance.

*Numerical values for the importance functions shown in Figs. 2 to 4 are available upon request.

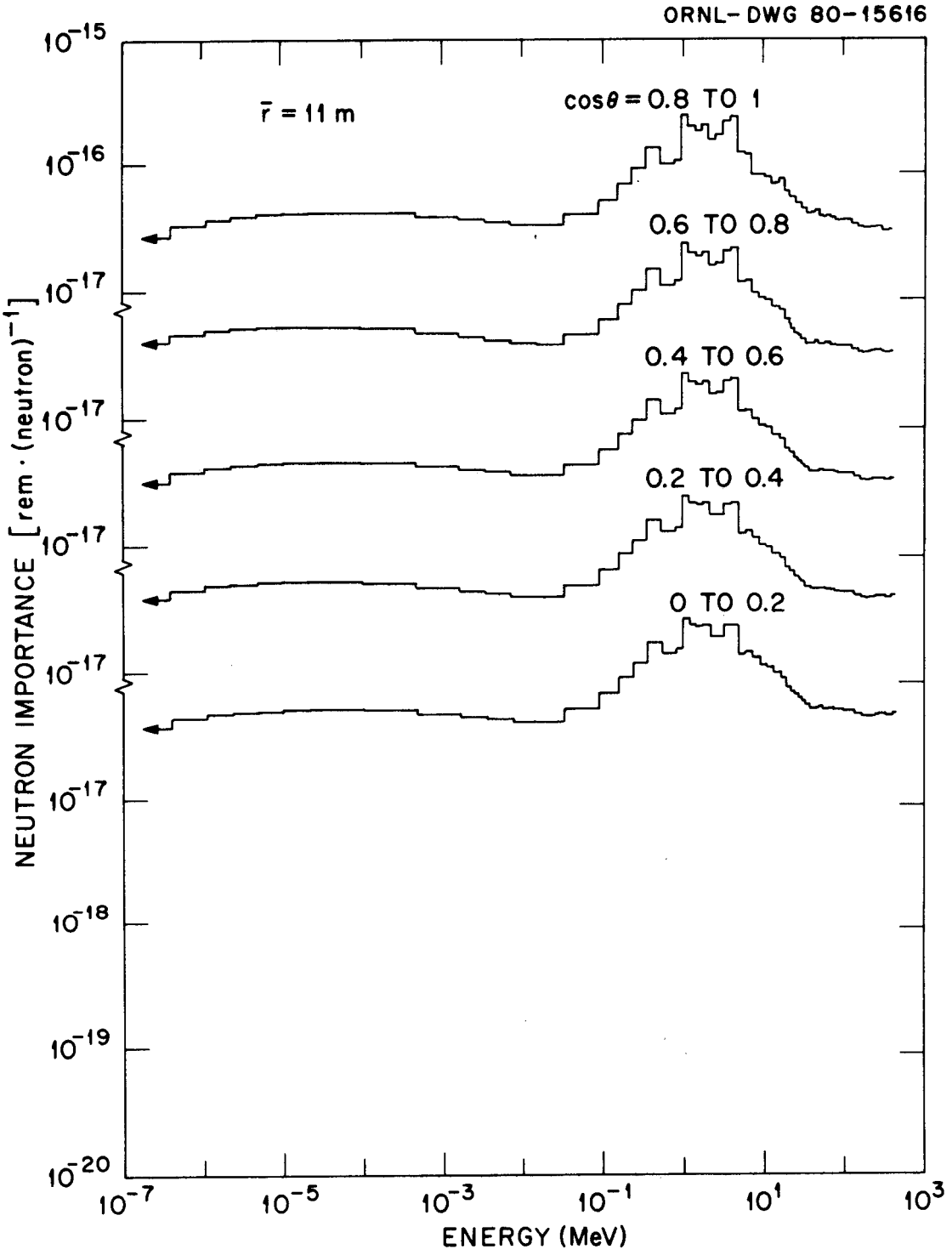

Fig. 2. Neutron importance vs. energy for various cosine intervals and for an average radial source to field point distance, $\bar{r}$, of 11 m.

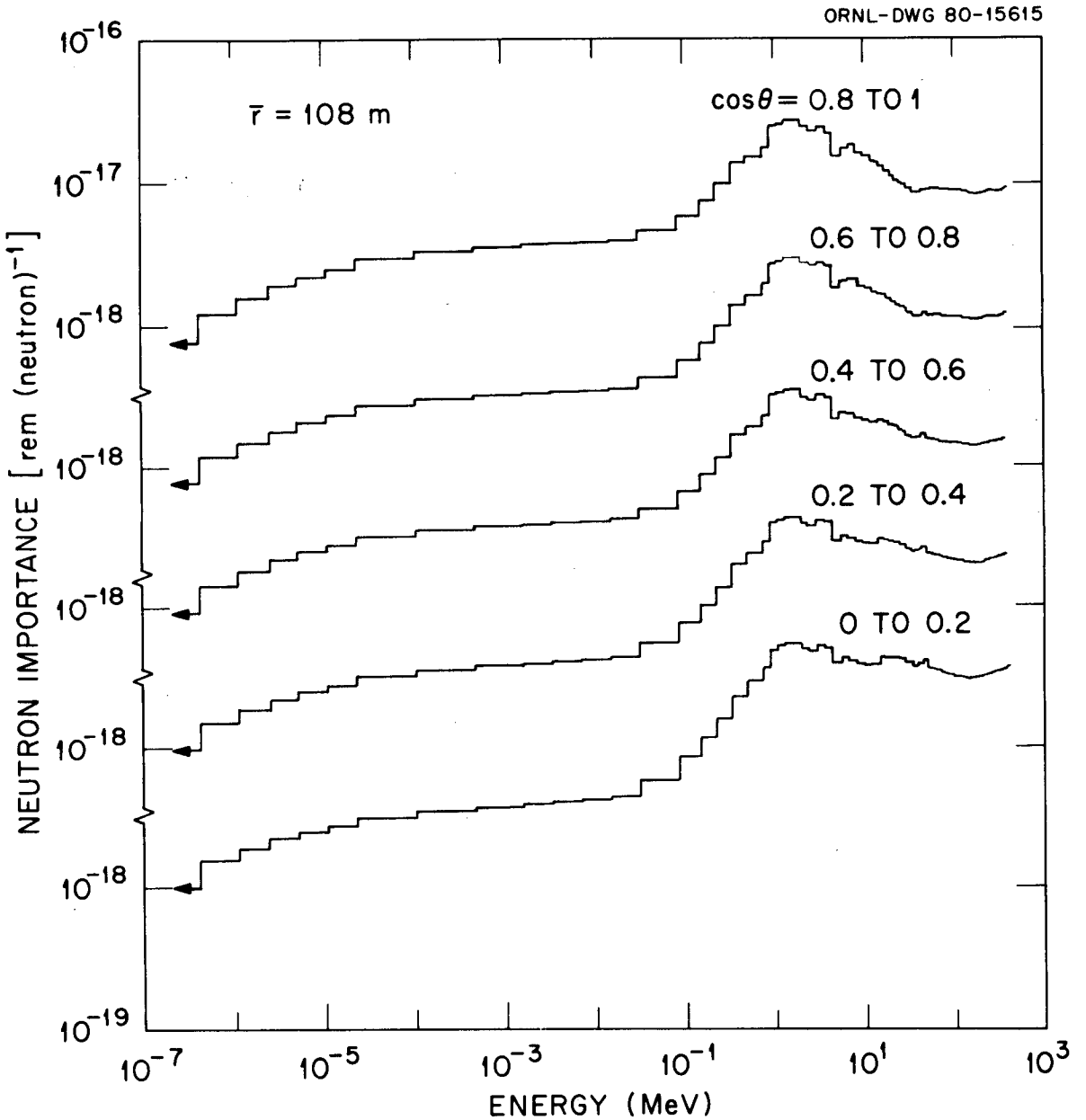

Fig. 3. Neutron importance vs. energy for various cosine intervals and for an average radial source-to-field point distance, $\bar{r}$, of 108 m.

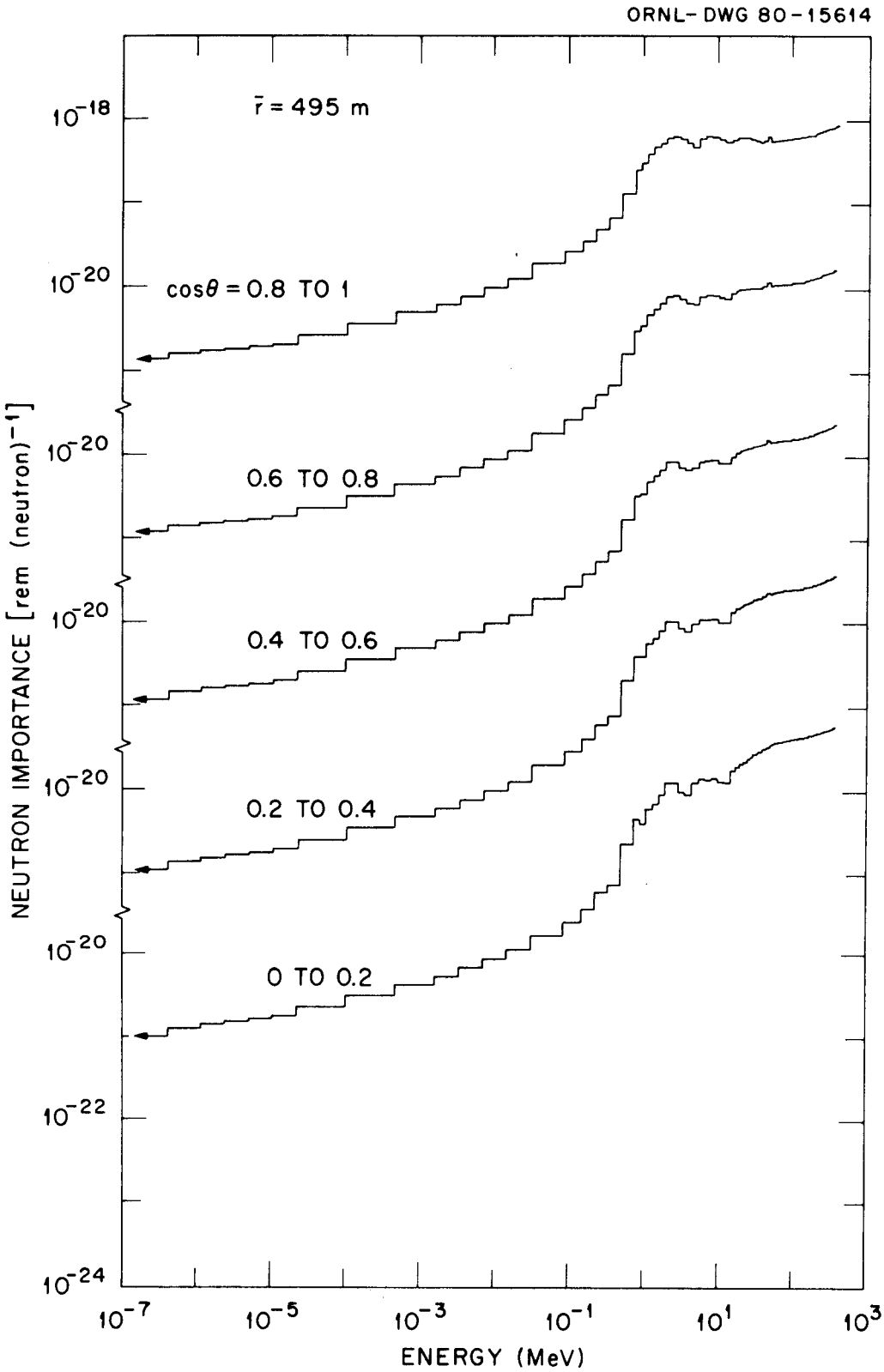

Fig. 4. Neutron importance vs. energy for various cosine intervals and for an average radial source-to-field point distance, $\bar{r}$, of 495 m.

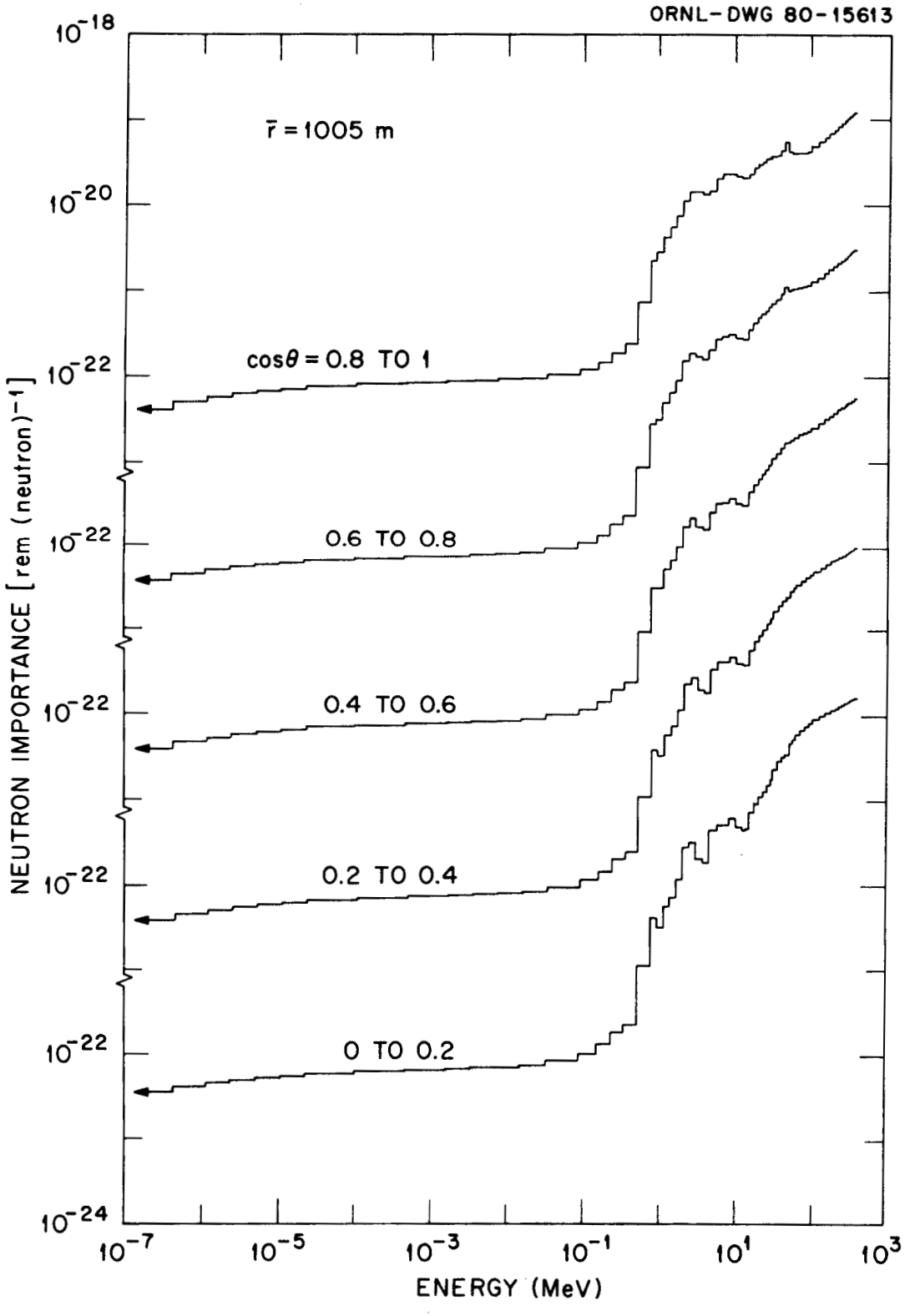

Fig. 5. Neutron importance vs. energy for various cosine intervals and for an average radial source-to-field point distance, $\bar{r}$, of 1005 m.

3 COMPARISONS WITH EXPERIMENTAL DATA

In this section calculated results using the neutron importance function of the previous sections are presented and compared with the experimental data of C. Distenfeld and D. Colvett.[2]

The dose equivalent as a function of $\bar{r}$ may be obtained from Eq. (1) if the source $S_i(E,\cos\Theta)$ is known. The energy distribution of the neutron source corresponding approximately to the experiment has been measured at energies $\gtrsim$ 20 MeV by R. Madey *et al.*,[17] and this measured spectrum is used here. The energy-angle distributions at energies $\gtrsim$ 20 MeV have also been measured by R. Madey and A. R. Baldwin*, and these distributions have also been used here. To carry out the calculation it is, of course, necessary to have the energy-angle distribution of neutrons from the source at energies $\leq$ 20 MeV. The assumption is made here that the energy distribution of low energy neutrons may be approximated by the energy distribution of neutrons produced by cosmic rays deep in the atmosphere+ and this low energy spectrum is smoothly joined to the spectrum above 20 MeV from Ref. 17. Furthermore, it is assumed that the low energy ($\leq$ 20 MeV) neutrons may be assumed to be isotropic, and it is assumed that there are no source photons.

---

*These energy-angle distributions are part of a doctoral dissertation being prepared at Kent State University, and are not yet published. We thank R. Madey and A. Baldwin for allowing us to use their results prior to publication.

+The actual low energy spectrum used is that calculated at 600 g/cm^2 in Ref. 18.

The calculated and experimental results are compared in Fig. 6. The calculated values are indicated by the solid circles. The horizontal bars on the calculated points indicate the radial distances over which the calculated results have been averaged. At $\overline{r}$ = 11 m the horizontal bars are not shown because they are smaller than the size of the points. The curve through the plotted points is drawn only to aid in comparing the calculated and experimental data. Because the experimental source normalization is uncertain (see below) the experimental data have been normalized to the calculated results at a radial distance of 600 m. At radial distances greater than approximately 150 m the calculated and experimental results are in very good agreement. At radial distances of 100 m and less the experimental data are somewhat higher than the calculated results. This discrepancy is probably due to the fact that the experimental source configuration is not a point, but is somewhat extended.[2]

In Ref. 2 it is estimated that the experimental source strength was 2×10^9 neutrons/s for neutrons with energy $\geq$ 20 MeV. The source strength below 20 MeV is not know. If the source spectrum used in the calculations, with the contribution from neutrons below 20 MeV obtained from the cosmic ray spectrum is used to obtain a normalization estimate for the experimental data, then the experimental points in Fig. 6 would be multiplied by approximately 2.5. Thus, on an absolute basis the calculated results are too low by approximately a factor of 2.5, but considering the very uncertain

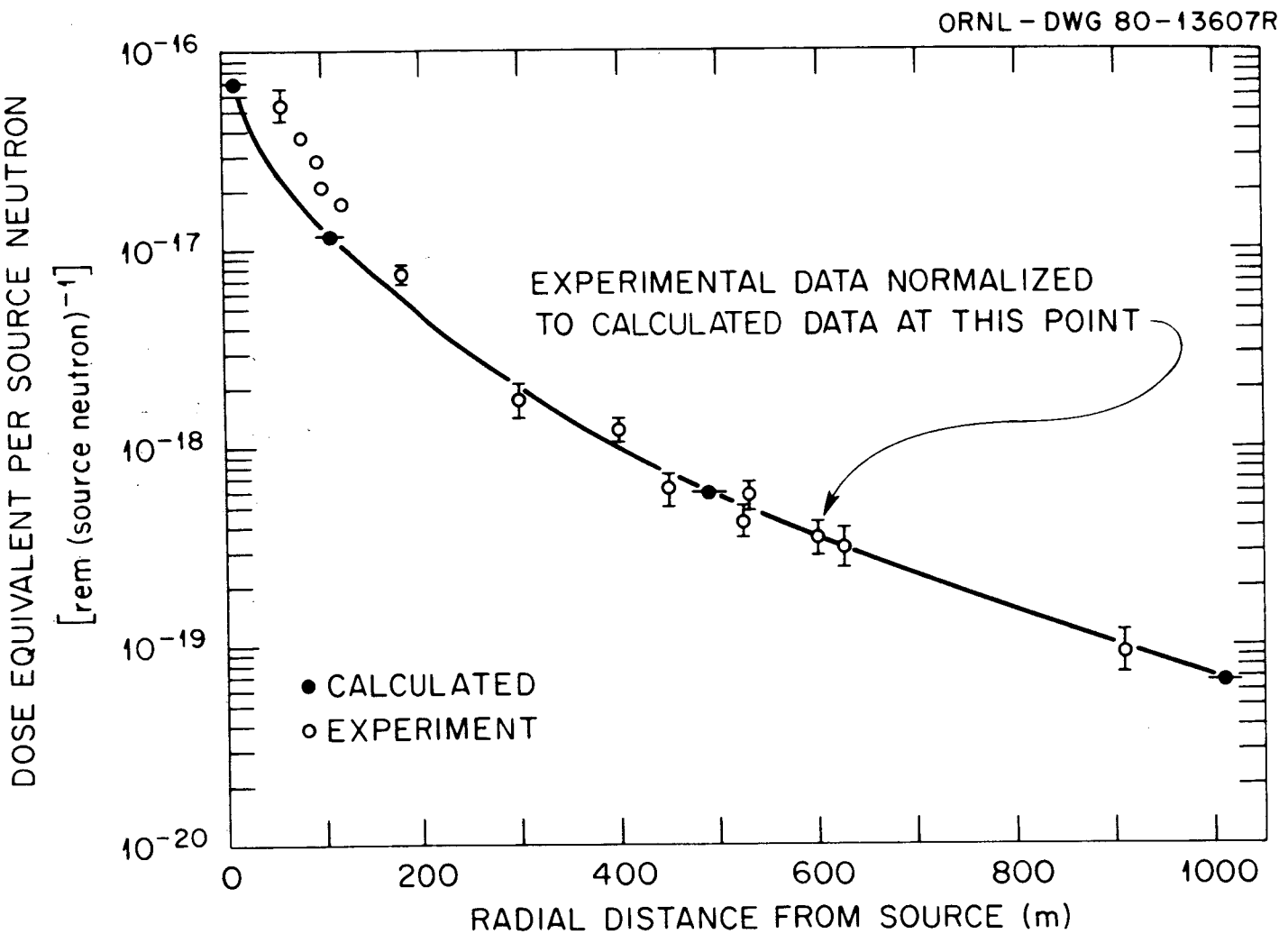

Fig. 6. Dose equivalent per unit source neutron vs. radial distance from the source.

neutron source normalization this discrepancy may not be real.

4 CALCULATIONS TO DETERMINE THE ROOF THICKNESS OVER A TARGET AREA FOR A 400 GEV PROTON ACCELERATOR

4.1 Neutron Source

In Fig. 7 a schematic diagram of the idealized geometry used in the source calculations is shown. The zero thickness proton beam is incident on a long (16 m) aluminum target that has a diameter of 0.004 m. In reality the target is a beam pipe and what is being considered are the protons that scrape the walls of this beam pipe. The concrete roof is 16 m long (parallel to target), 32 m wide (transverse to target) and of variable thickness. Reflectional symmetry is assumed with respect to the y-z plane at x = 0. This symmetry assumption is an idealization to improve the statistical accuracy of the Monte Carlo calculations, i.e., neutrons are scored through both "roofs" and one-half of this number is assumed to be emitted through the actual roof. In reality, of course, there is a floor 5 m below the target. The walls of the target area are not shown in Fig. 7 and are neglected in the calculations. It is assumed that these walls are sufficiently thick that they absorb essentially all of the radiation that strikes them. It is further assumed that the albedo from the floor and walls that enter the roof may be neglected.

The transport calculations to obtain the energy-angle and spatial distribution of the neutrons that emerge from the

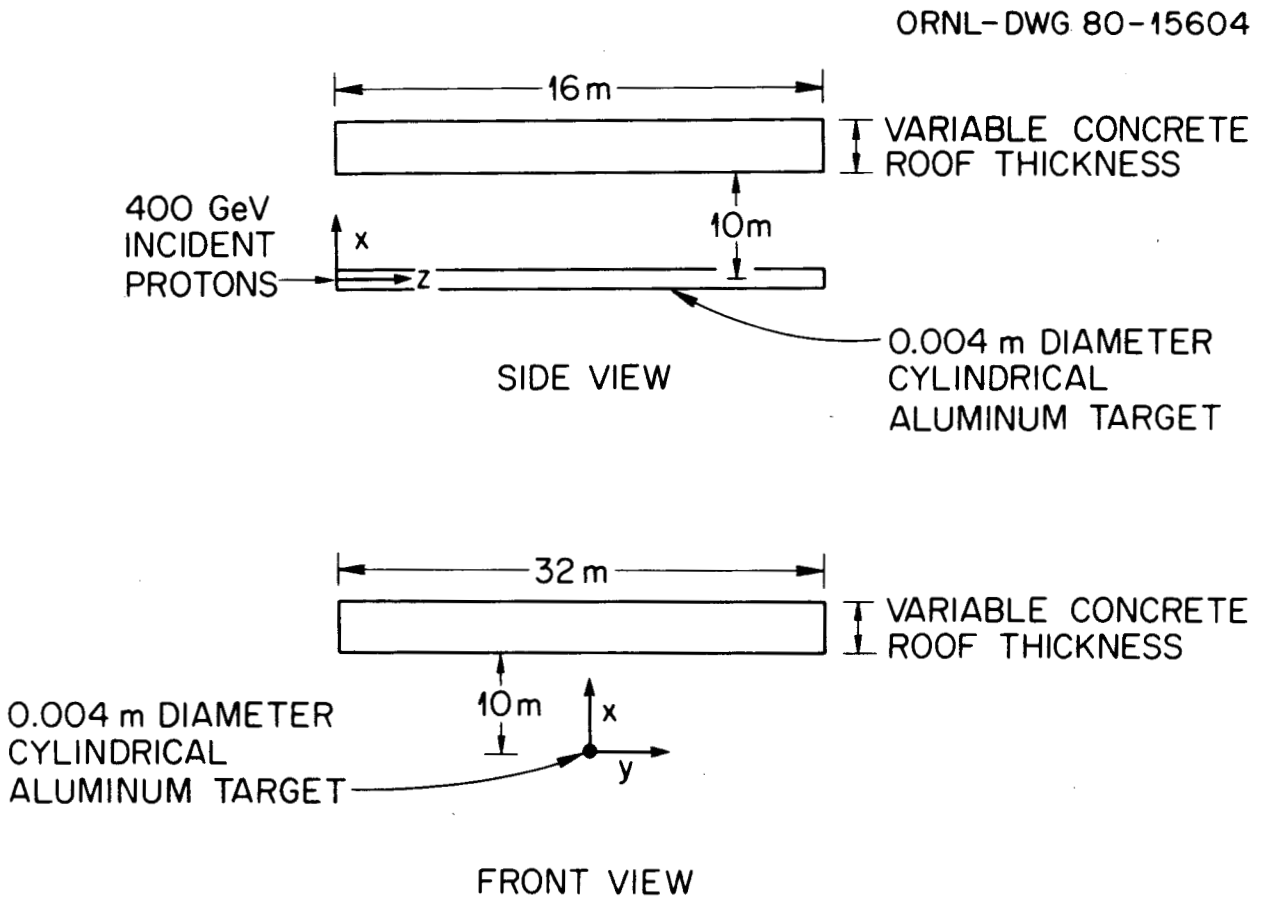

REFLECTIONAL SYMMETRY ABOUT y-z PLANE AT x=0 IS ASSUMED

DRAWING NOT TO SCALE

Fig. 7. Schematic diagram of the geometry used to calculate the energy-angle distribution of neutrons through the roof of a 400 GeV proton accelerator target area.

roof as a function of roof thickness were carried out with the high-energy transport code HETC[19] and the low energy ($\leq$ 15 MeV) transport code MORSE.[20] The code HETC has been described in detail elsewhere so only a brief discussion will be given here.[21] This code contains differential particle production cross sections for nucleon-nculeus and pion-nucleus collisions at all energies $\geq$ 15 MeV. With this cross section data and a variety of other physical data such as charged particle stopping powers, the code treats the nucleon-meson cascade that occurs when high-energy particles pass through matter. The code utilizes Monte Carlo techniques and is capable of treating essentially arbitrary geometry. When neutrons fall below 15 MeV they are transported by the Monte Carlo code MORSE. The cross section data utilized in MORSE was taken from Ref. 10.

Calculations have been carried out for roof thicknesses of 0.0, .3, .6, .9, and 1.2 m. The energy-angle distribution of neutrons emerging from the roof as a function of spatial position and the angular distribution of these neutrons is not azimuthally symmetric. Therefore, these distributions cannot directly be used in conjunction with the importance functions presented earlier in this paper. To make the distributions useable they have been averaged over the spatial extent of the roof and have been averaged over azimuthal angles. This azimuthal averaging is consistent with possible beam losses occuring in each of the two counter-rotating beams passing through the experimental hall. The energy distribu-

tions of the neutrons in various cosine intervals are shown in Fig. 8 for a roof thickness of .6 m. The distributions for the other roof thicknesses are similar to those shown in Fig. 8.

Because of the averaging discussed above the skyshine results based on the neutron distributions such as that shown in Fig. 8 are approximate. However, at the energies considered here, the major uncertainties in the results arise from the uncertainties in the differential partial production cross section. There are very little data on such cross sections and the data that do exist are primarily restricted to very small angles rather than to the large angles of interest here. In addition to HETC, there is another code, CASIM[22] that is capable of doing high-energy transport calculations.* Both codes use differential particle production cross sections based on the small amount of available data, but the methods used are quite different and therefore it is instructive to compare results obtained with the two codes.

In Fig. 9 the total number of nonelastic collisions produced in specified volumes of the roof (see Fig. 7) by neutrons, protons, and charged pions with momentum $\geq$ 300 MeV/c as obtained with HETC and with CASIM are compared. The momenta of particles considered is restricted to $\geq$ 300 MeV/c because CASIM does not treat the lower energy particles. In the figure the number of nonelastic collisions in volumes

*All of the CASIM results were obtained by Dr. P. Gollon of the Brookhaven National Laboratory and the comparison between the HETC and CASIM results were done in collaboration with Dr. Gollon.

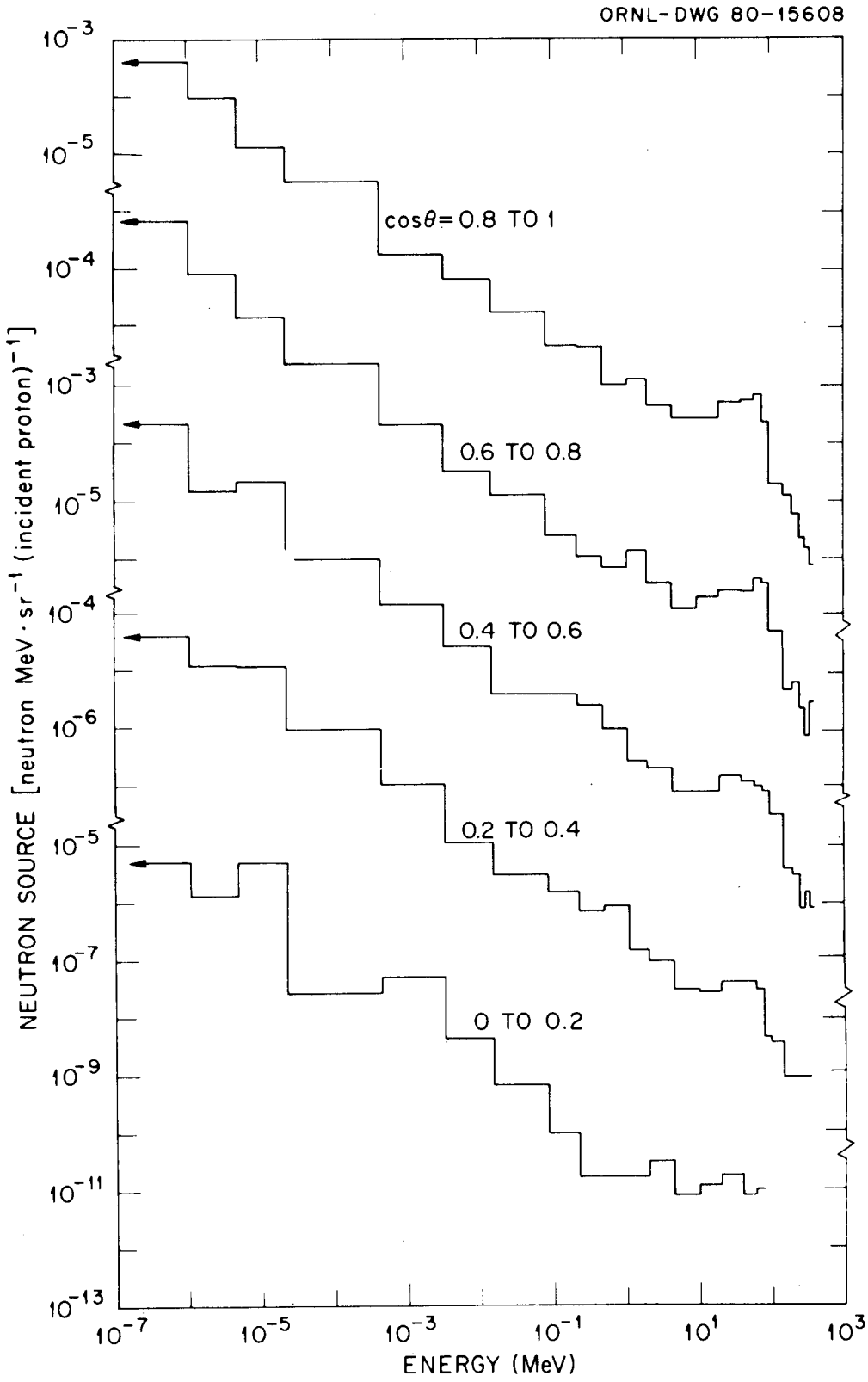

Fig. 8. Number of neutrons per unit energy per unit solid angle per incident proton vs. energy in the specified cosine intervals emitted through the roof in the configuration shown in Fig. 1 for a roof thickness of .6 m.

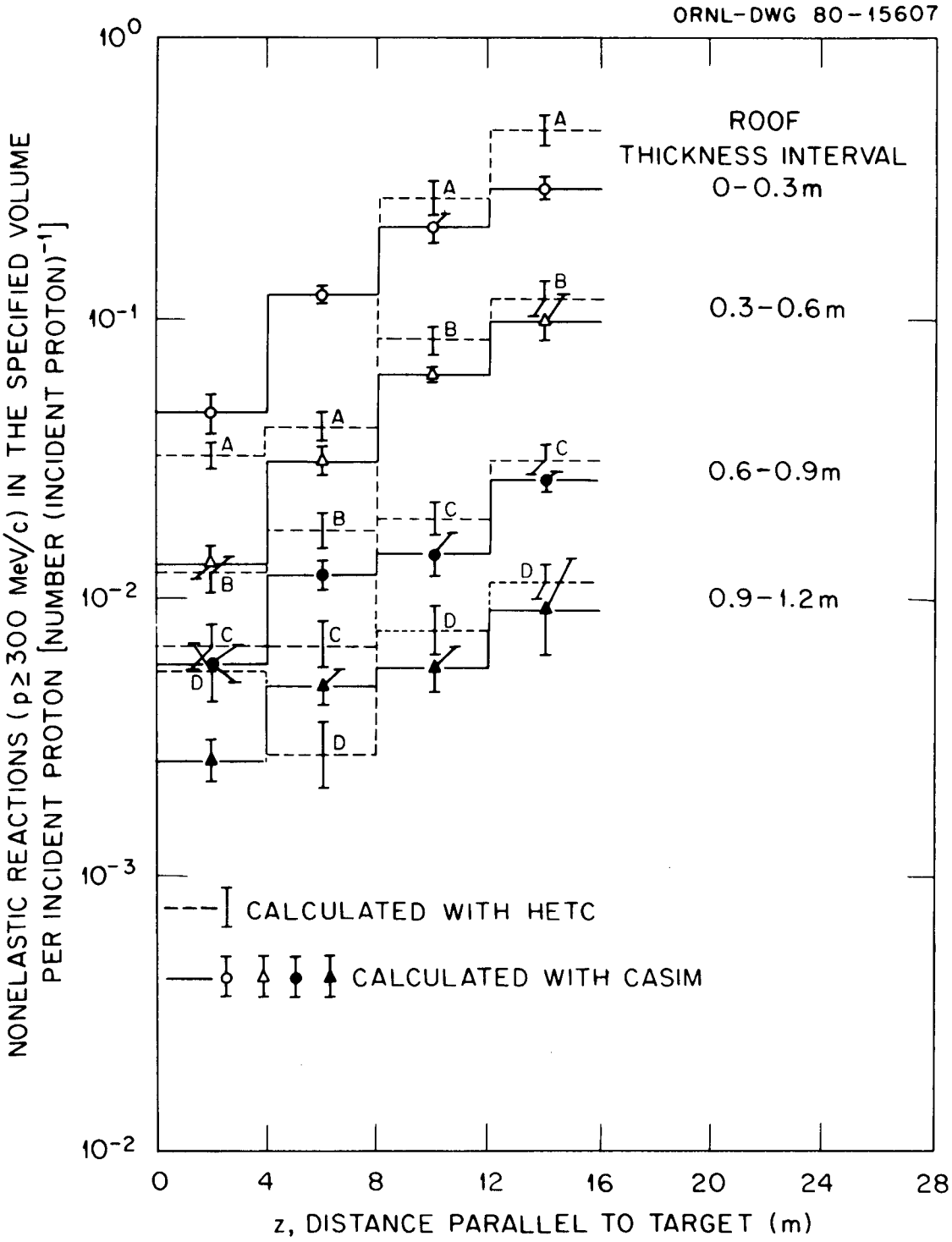

Fig. 9. Comparison between calculated results obtained with HETC and CASIM for the number of nonelastic collisions per incident 400 GeV proton (see Fig. 7) in specified volume intervals of the concrete roof. The nonelastic collisions considered are all of those produced by neutrons, protons, and charged pions with momenta $\geq$ 300 MeV/c.

specified by roof thickness intervals, z intervals, and the entire width of the roof are compared. The errors in all cases are statistical and represent one standard deviation in the Monte Carlo calculations. As the figure indicates the agreement between the two calculations is reasonable in almost all volume intervals. This agreement does not provide any certainty that the results are correct, but it does indicate that two independent estimates based on the available data are in agreement.

4.2 Dose Equivalent vs. Radial Distance from the Source for Various Roof Thicknesses

With the approximated neutron source distribution discussed in Section 4.1, and the adjoint results discussed in Section 2, it is straightforward to calculate the dose equivalent at the air-ground interface as a function of radial distance from the (point) source for various roof thicknesses. It is to be noted that the additional approximation is made here that the source is always 15 m above the ground. Actually, the roof begins at 15 m above the ground (the roof begins at 10 m above the target and the target is 5 m above the ground or floor so for a roof thickness > 0 m there is a slight approximation in placing the source.

Calculated results for roof thicknesses of 0, .3, .6, .9, and 1.2 m are shown in Fig. 10. The solid points show the calculated results from Eq. (1). The solid curves are drawn through the points only as an aid to interpret the

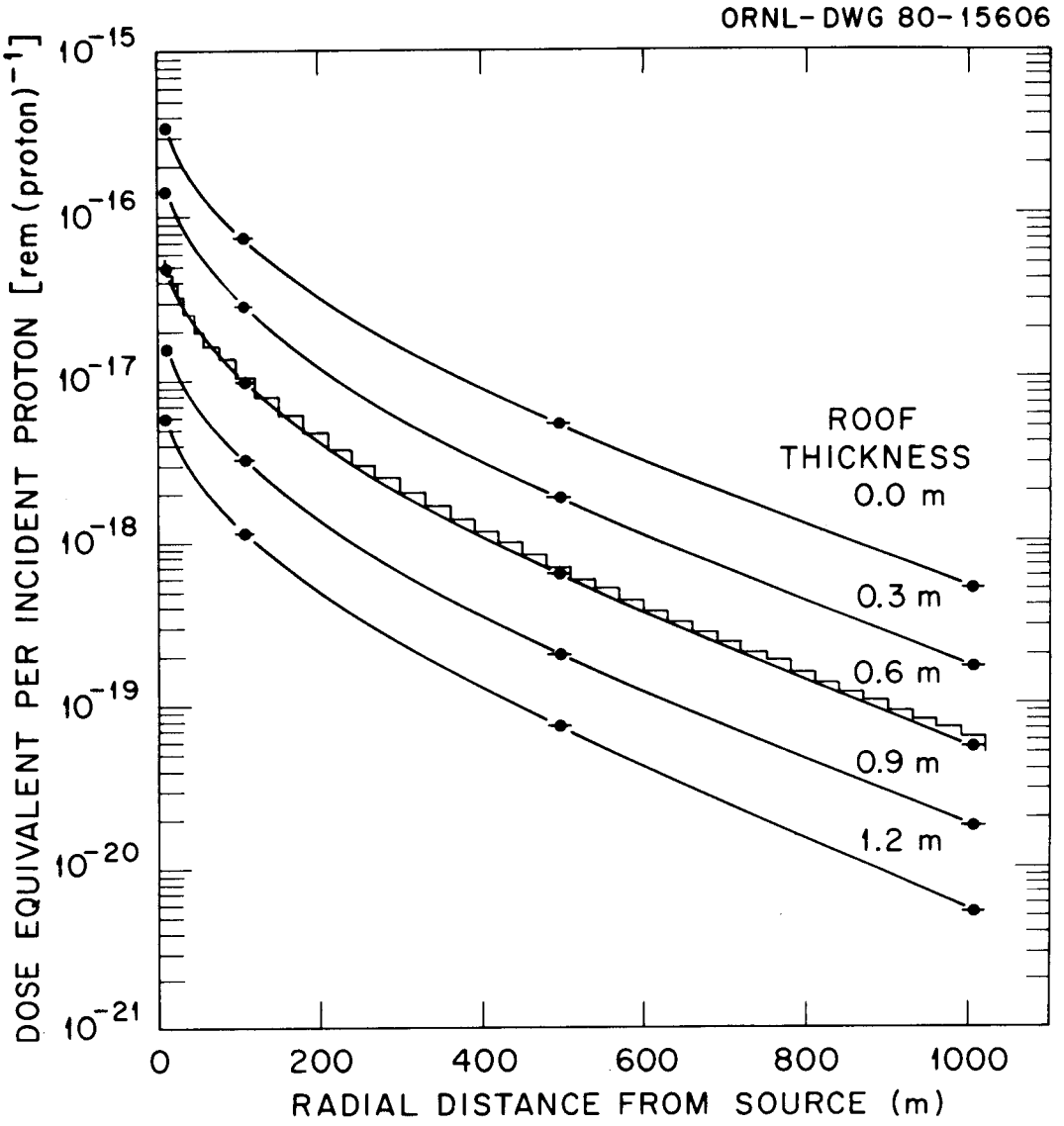

Fig. 10. Dose equivalent per incident proton vs. radial distance from the source for various roof thicknesses.

results. The horizontal bars on the points are to indicate the spatial intervals over which the points have been averaged due to the finite difference calculations. At a radial distance of 11 m the bars are not shown because they are smaller than the plotted points. In considering the figure, it should be remembered that the values at the smaller radial distances are idealized in the sense that the roof itself would shadow this region and because of the assumption of a point source this shadowing effect is not included in the calculations.

Adjoint methods as used in obtaining the curves in Fig. 10 are powerful in that similar curves for a large variety of energy-angle source distributions may easily be obtained. On the other hand, such methods provide the dose equivalent at only a small number of points. Forward, i.e., non-adjoint, calculations provide the dose equivalent at a large number of points for a specific source.

For the case of the .6 m thick roof, forward calculations have been carried out using all of the same assumptions and cross section data as in the adjoint calculation. The results of this calculation are shown as the histogram in Fig. 10. In principle, forward and adjoint calculations should agree exactly, i.e., the histogram should go through the solid points for the .6 m thickness case, but this is not true in practice. The slight differences between the two results shown in the figure arise because the numerical approximation used in the forward and adjoint calculations are not precisely the same.

These slight differences are not significant for most applications.

The dose equivalent results in Fig. 10 apply at the air-ground interface, or more precisely, have been averaged over a 1 m interval in the air immediately adjacent to the ground. The variation of the dose equivalent with distance away from the ground is of some interest and is available from the forward calculations for the 60 cm thick roof. This dose equivalent is shown in Fig. 11 as a function of distance from the ground for several values of $\bar{r}$. Results are shown out to 28 m above the ground. The source is 15 m above the ground so the results shown are both above and below the source. As the figure indicates the dose equivalent is changing only very slowly over the height intervals shown. Also shown in the figure for comparative purposes are the dose equivalent values obtained from the adjoint calculations. The same minor discrepancies between the forward and adjoint calculations that were discussed in conjunction with Fig. 10 also appear in Fig. 11.

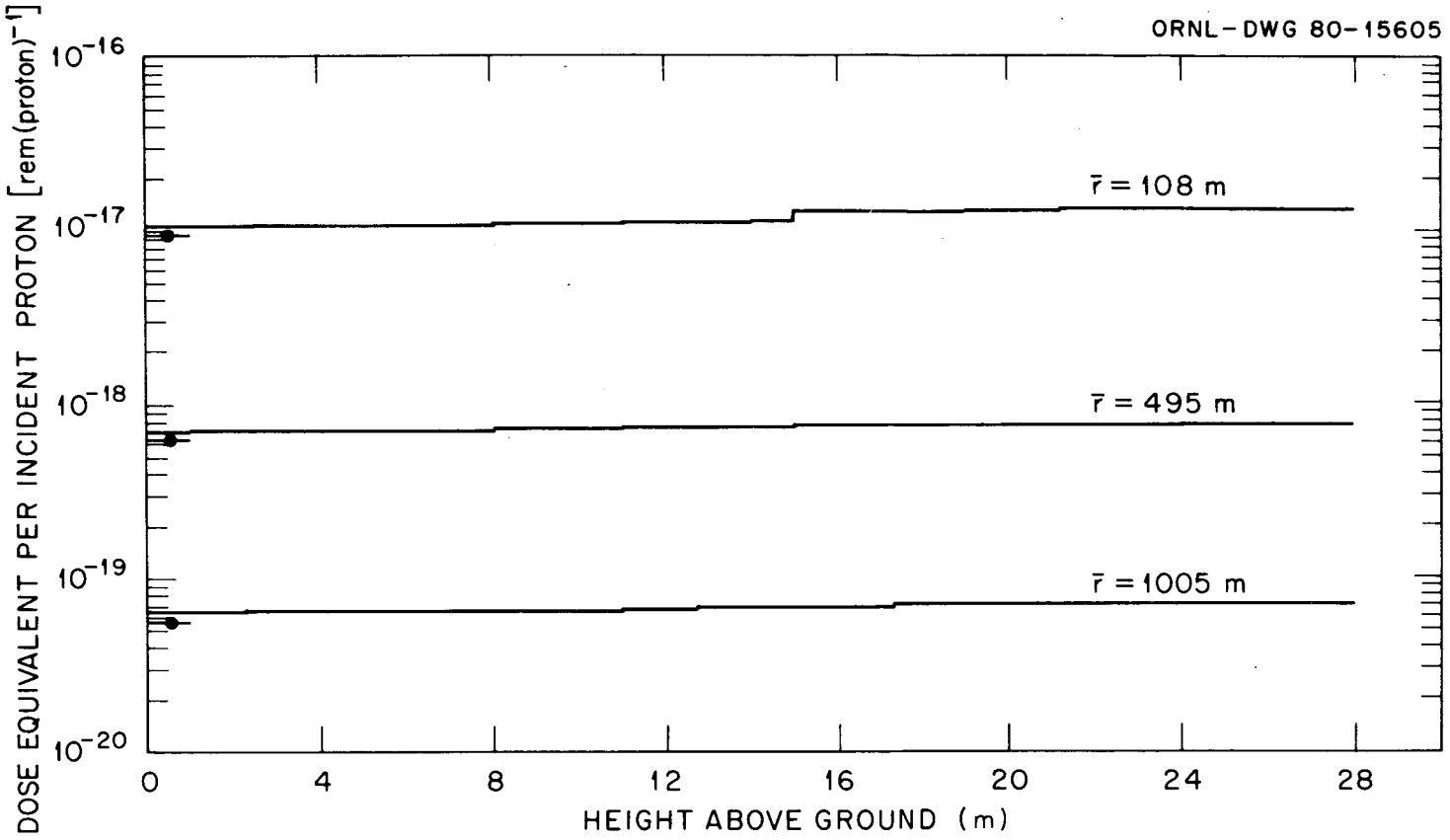

Fig. 11. Dose equivalent per incident proton vs. height above the ground for various values of $\bar{r}$ and for a roof thickness of .6 m.

APPENDIX A

A photon importance function (see Eq. (1)) is obtained as part of the adjoint calculations. This importance function was not used in the body of the paper and therefore was not shown. For some applications it may be of interest, and therefore it is presented in this appendix.

In Fig. A.1 to A.4 the photon importance is given as a function of energy for various cosine intervals and for $\bar{r}$ = 11, 108, 495, and 1005 m. Numerical values for the photon importance shown in Fig. A.1 to A.4 are available upon request.

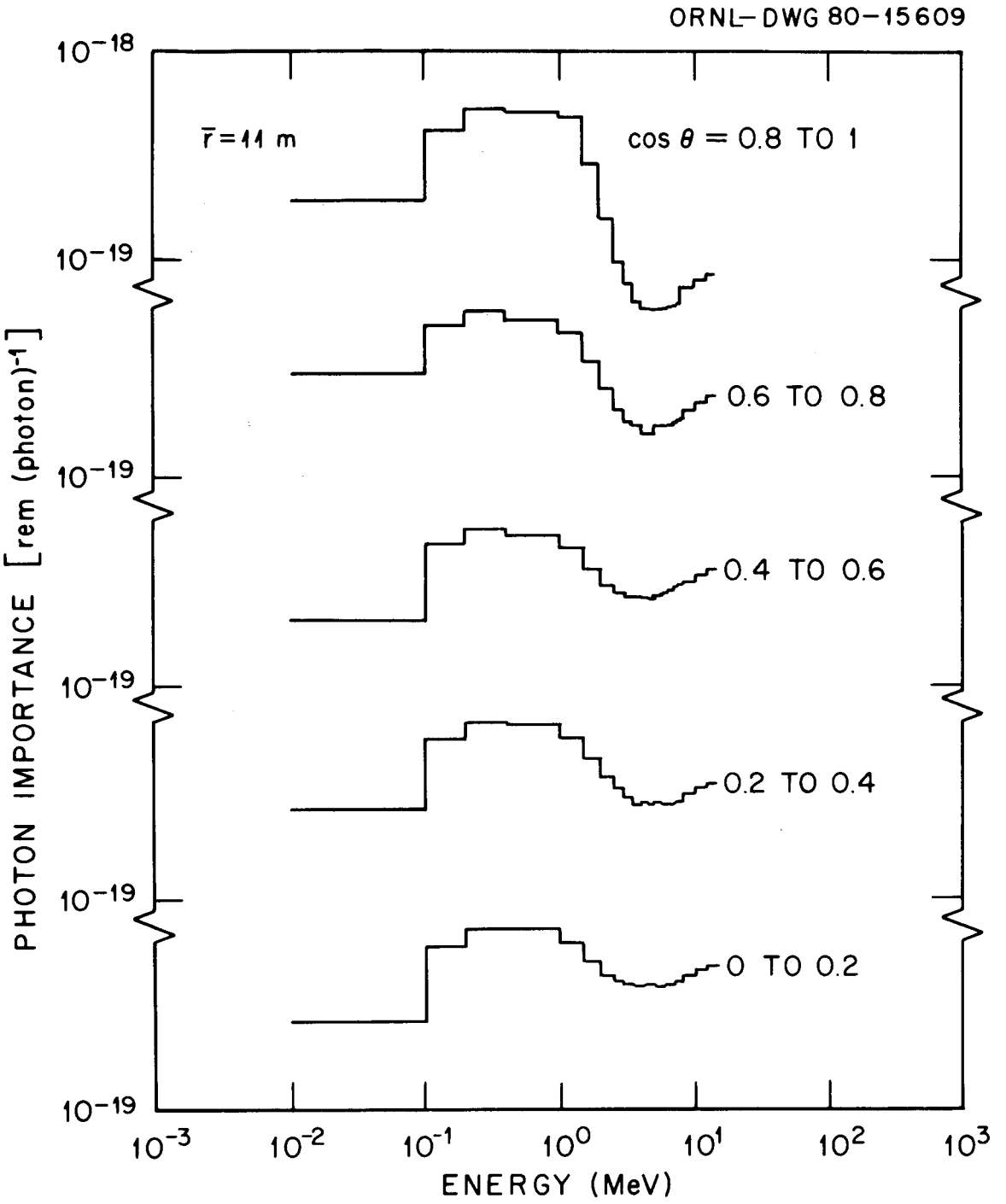

Fig. A.1. Photon importance vs. energy for various cosine intervals and for an average radial source-to-field point distance, $\bar{r}$, of 11 m.

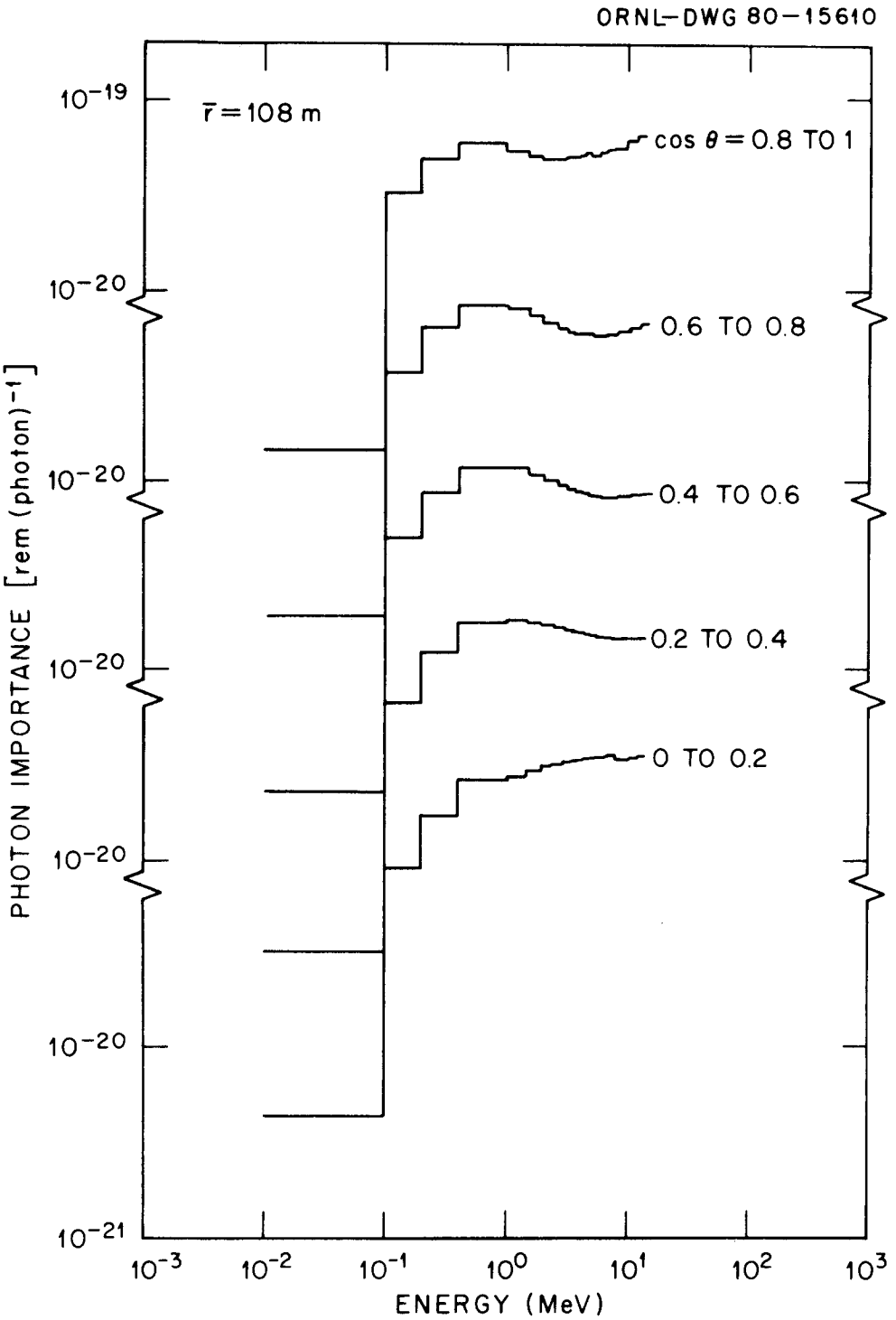

Fig. A.2. Photon importance vs. energy for various cosine intervals and for an average radial source-to-field point distance, $\bar{r}$, of 108 m.

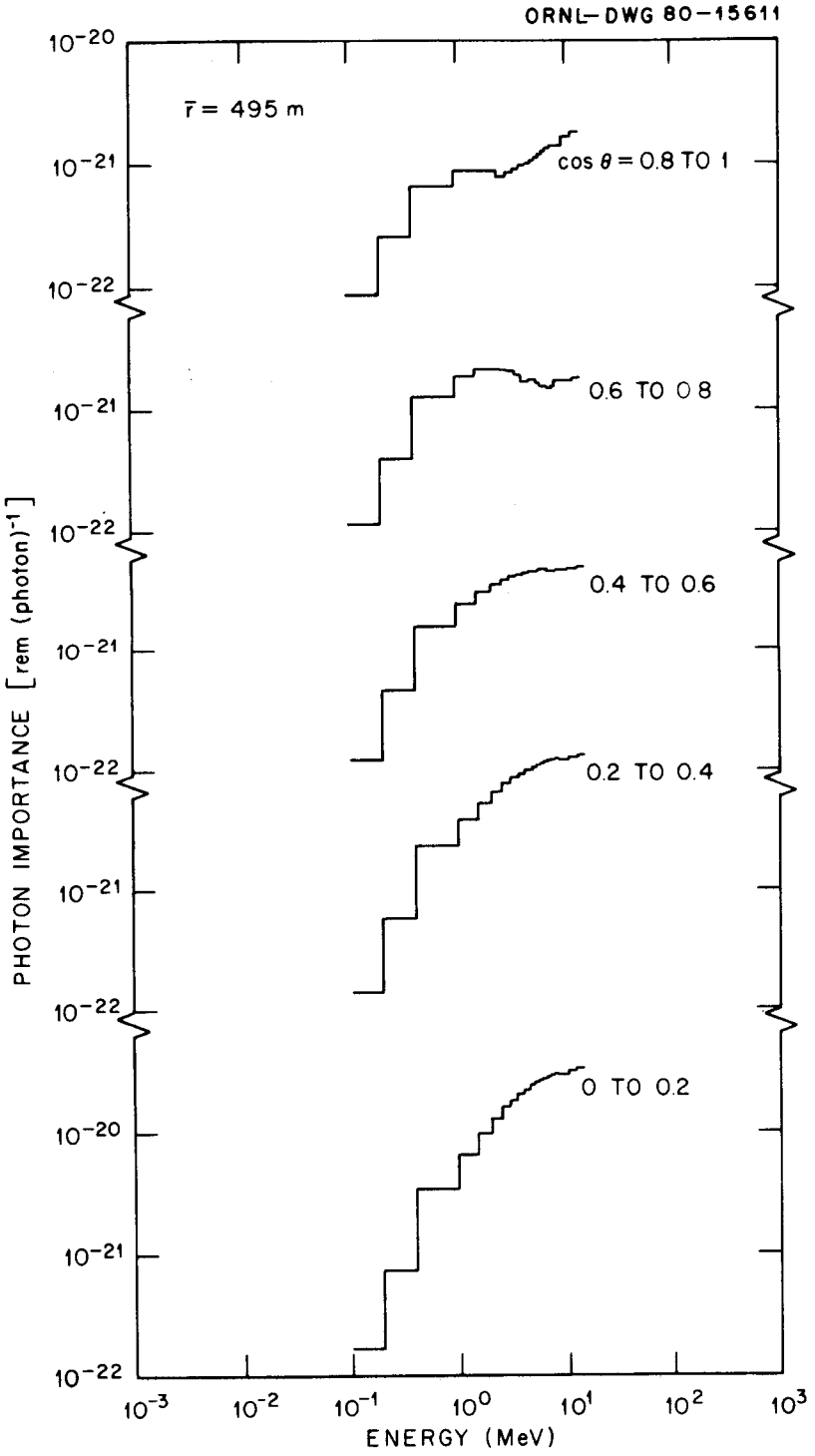

Fig. A.3. Photon importance vs. energy for various cosine intervals and for an average radial source-to-field point distance, $\bar{r}$, of 495 m.

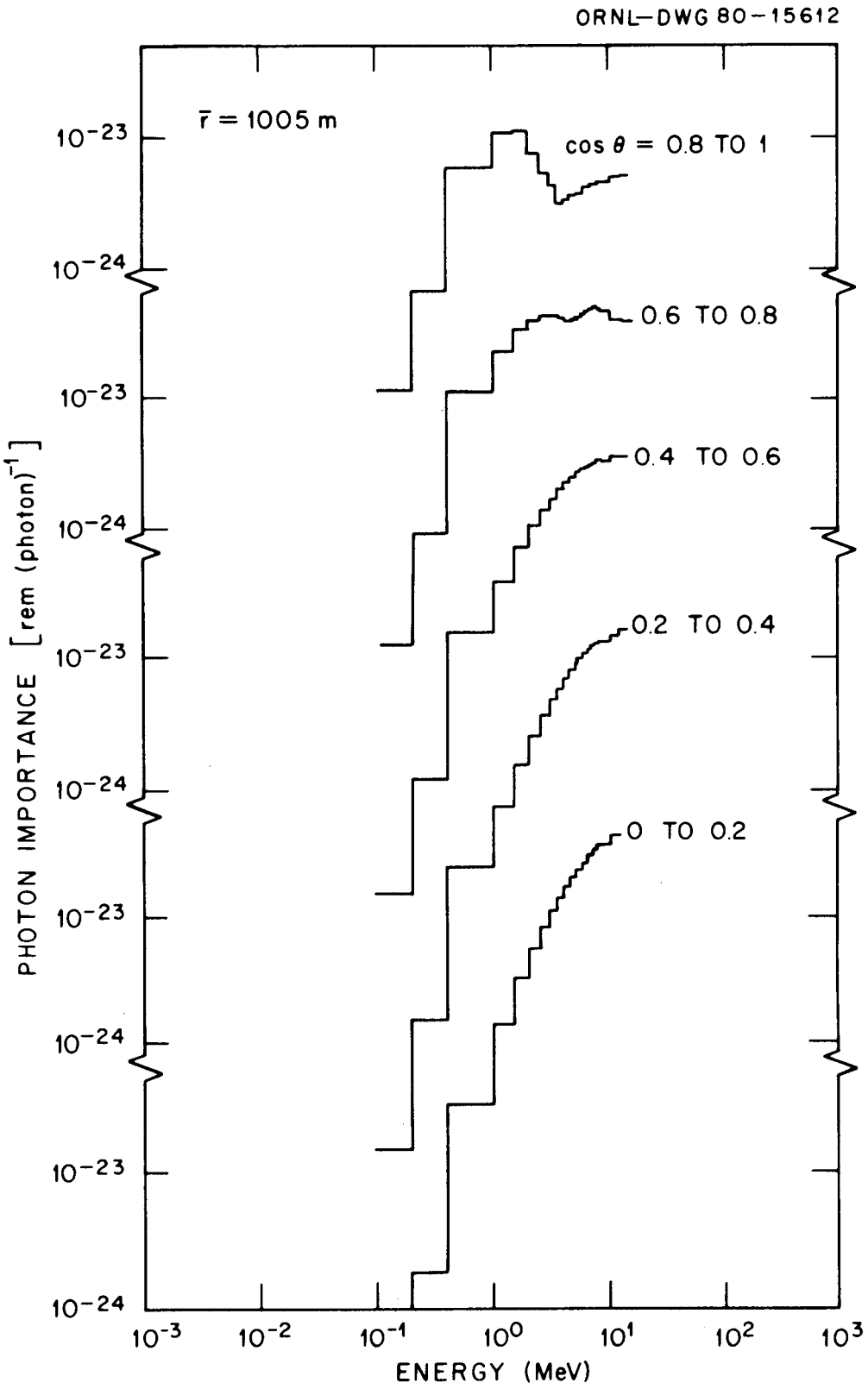

Fig. A.4. Photon importance vs. energy for various cosine intervals and for an average radial source-to-field point distance, $\bar{r}$, of 1005 m.

APPENDIX B

Numerical Values of the Importance Function

In Figs. 2 to 5 and A.1 to A.4 the importance function for neutrons and photons, respectively, are shown as a function of energy in specified cosine intervals. In this appendix the numerical values of the importance functions from which the histograms were drawn are given.

In Tables B.1 to B.4 the neutron importance is given as a function of energy for the specified cosine intervals and for $\bar{r}$ = 11, 108, 495 and 1005 m, respectively. In Tables B.5 to B.8 similar results are given for the photon importance.

TABLE B.1

Neutron Importance vs. Energy for Specified Cosine Intervals and $\bar{r}$ = 11 m

E_{High} (MeV)	E_{Low} (MeV)	Neutron Importance [Rem (Neu.)$^{-1}$] cosθ = 0 to .2	cosθ = .2 to .4	cosθ = .4 to .6	cosθ = .6 to .8	cosθ = .8 to 1
4.00E+02	3.75E+02	5.33E-17	4.94E-17	4.06E-17	3.88E-17	3.52E-17
3.75E+02	3.50E+02	5.16E-17	4.78E-17	3.93E-17	3.78E-17	3.48E-17
3.50E+02	3.25E+02	5.14E-17	4.75E-17	3.92E-17	3.78E-17	3.53E-17
3.25E+02	3.00E+02	5.16E-17	4.78E-17	3.94E-17	3.82E-17	3.59E-17
3.00E+02	2.75E+02	5.26E-17	4.87E-17	4.03E-17	3.92E-17	3.70E-17
2.75E+02	2.50E+02	5.30E-17	4.92E-17	4.09E-17	3.97E-17	3.76E-17
2.50E+02	2.25E+02	5.20E-17	4.83E-17	4.01E-17	3.91E-17	3.71E-17
2.25E+02	2.00E+02	5.08E-17	4.72E-17	3.91E-17	3.82E-17	3.65E-17
2.00E+02	1.75E+02	5.04E-17	4.69E-17	3.89E-17	3.81E-17	3.65E-17
1.75E+02	1.50E+02	5.10E-17	4.75E-17	3.96E-17	3.88E-17	3.73E-17
1.50E+02	1.25E+02	5.27E-17	4.91E-17	4.12E-17	4.04E-17	3.91E-17
1.25E+02	1.00E+02	5.54E-17	5.17E-17	4.36E-17	4.28E-17	4.19E-17
1.00E+02	9.00E+01	5.53E-17	5.18E-17	4.39E-17	4.27E-17	4.09E-17
9.00E+01	8.00E+01	5.56E-17	5.20E-17	4.40E-17	4.28E-17	4.15E-17
8.00E+01	7.00E+01	5.63E-17	5.25E-17	4.46E-17	4.34E-17	4.26E-17
7.00E+01	6.00E+01	5.80E-17	5.41E-17	4.61E-17	4.50E-17	4.49E-17
6.00E+01	5.50E+01	5.68E-17	5.29E-17	4.53E-17	4.37E-17	4.33E-17
5.50E+01	5.00E+01	5.74E-17	5.34E-17	4.57E-17	4.43E-17	4.45E-17
5.00E+01	4.50E+01	5.97E-17	5.55E-17	4.67E-17	4.60E-17	4.88E-17
4.50E+01	4.00E+01	5.65E-17	5.25E-17	4.45E-17	4.38E-17	4.65E-17
4.00E+01	3.50E+01	5.64E-17	5.24E-17	4.45E-17	4.37E-17	4.57E-17
3.50E+01	3.00E+01	6.10E-17	5.69E-17	4.82E-17	4.76E-17	5.02E-17
3.00E+01	2.75E+01	6.57E-17	6.14E-17	5.22E-17	5.15E-17	5.44E-17
2.75E+01	2.50E+01	6.80E-17	6.36E-17	5.37E-17	5.31E-17	5.57E-17
2.50E+01	2.25E+01	7.25E-17	6.81E-17	5.76E-17	5.74E-17	6.06E-17
2.25E+01	2.00E+01	7.83E-17	7.37E-17	6.24E-17	6.23E-17	6.52E-17
2.00E+01	1.75E+01	8.46E-17	7.98E-17	6.73E-17	6.70E-17	6.82E-17
1.75E+01	1.49E+01	9.83E-17	9.36E-17	8.07E-17	8.15E-17	8.53E-17
1.49E+01	1.35E+01	1.08E-16	1.03E-16	8.48E-17	8.49E-17	7.95E-17
1.35E+01	1.22E+01	1.10E-16	1.04E-16	8.61E-17	8.55E-17	7.82E-17
1.22E+01	1.00E+01	1.22E-16	1.15E-16	9.79E-17	9.65E-17	8.76E-17
1.00E+01	8.19E+00	1.26E-16	1.20E-16	1.03E-16	1.01E-16	9.23E-17
8.19E+00	6.70E+00	1.44E-16	1.36E-16	1.16E-16	1.11E-16	9.12E-17
6.70E+00	5.49E+00	1.58E-16	1.52E-16	1.35E-16	1.35E-16	1.31E-16
5.49E+00	4.49E+00	1.51E-16	1.46E-16	1.32E-16	1.33E-16	1.34E-16
4.49E+00	3.68E+00	2.58E-16	2.55E-16	2.38E-16	2.46E-16	2.58E-16
3.68E+00	3.01E+00	2.53E-16	2.48E-16	2.30E-16	2.34E-16	2.39E-16
3.01E+00	2.47E+00	2.06E-16	2.01E-16	1.83E-16	1.85E-16	1.84E-16
2.47E+00	2.02E+00	2.08E-16	2.01E-16	1.79E-16	1.79E-16	1.69E-16
2.02E+00	1.65E+00	2.58E-16	2.52E-16	2.26E-16	2.29E-16	2.22E-16
1.65E+00	1.35E+00	2.50E-16	2.43E-16	2.11E-16	2.12E-16	1.96E-16
1.35E+00	1.11E+00	2.56E-16	2.50E-16	2.21E-16	2.25E-16	2.15E-16
1.11E+00	9.07E-01	2.86E-16	2.83E-16	2.61E-16	2.70E-16	2.68E-16
9.07E-01	7.43E-01	1.65E-16	1.58E-16	1.35E-16	1.33E-16	1.15E-16
7.43E-01	4.98E-01	1.52E-16	1.47E-16	1.25E-16	1.25E-16	1.09E-16
4.98E-01	3.34E-01	1.84E-16	1.81E-16	1.59E-16	1.66E-16	1.45E-16
3.34E-01	2.24E-01	1.27E-16	1.25E-16	1.11E-16	1.13E-16	9.91E-17
2.24E-01	1.50E-01	9.80E-17	9.60E-17	8.43E-17	8.65E-17	7.44E-17
1.50E-01	8.65E-02	7.33E-17	7.21E-17	6.31E-17	6.52E-17	5.55E-17
8.65E-02	3.18E-02	5.43E-17	5.42E-17	4.82E-17	5.03E-17	4.28E-17
3.18E-02	1.50E-02	4.32E-17	4.37E-17	3.93E-17	4.15E-17	3.52E-17
1.50E-02	7.10E-03	4.30E-17	4.38E-17	3.94E-17	4.21E-17	3.55E-17
7.10E-03	3.35E-03	4.48E-17	4.58E-17	4.11E-17	4.44E-17	3.70E-17
3.35E-03	1.58E-03	4.68E-17	4.80E-17	4.28E-17	4.69E-17	3.85E-17
1.58E-03	4.54E-04	4.91E-17	5.06E-17	4.49E-17	5.01E-17	4.04E-17
4.54E-04	1.01E-04	5.21E-17	5.40E-17	4.74E-17	5.40E-17	4.26E-17
1.01E-04	2.26E-05	5.29E-17	5.49E-17	4.79E-17	5.54E-17	4.29E-17
2.26E-05	1.07E-05	5.20E-17	5.40E-17	4.68E-17	5.46E-17	4.17E-17
1.07E-05	5.04E-06	5.10E-17	5.30E-17	4.57E-17	5.37E-17	4.07E-17
5.04E-06	2.38E-06	4.97E-17	5.16E-17	4.43E-17	5.23E-17	3.92E-17
2.38E-06	1.13E-06	4.76E-17	4.93E-17	4.20E-17	5.01E-17	3.70E-17
1.13E-06	4.14E-07	4.41E-17	4.56E-17	3.83E-17	4.65E-17	3.35E-17
4.14E-07	1.00E-10	3.72E-17	3.88E-17	3.17E-17	4.03E-17	2.74E-17

TABLE B.2

Neutron Importance vs. Energy for Specified Cosine Intervals and $\bar{r}$ = 108 m

E_{High} (MeV)	E_{Low} (MeV)	Neutron Importance [Rem (Neu.)$^{-1}$] cosθ = 0 to .2	cosθ = .2 to .4	cosθ = .4 to .6	cosθ = .6 to .8	cosθ = .8 to 1
4.00E+02	3.75E+02	3.75E-17	2.36E-17	1.58E-17	1.26E-17	9.34E-18
3.75E+02	3.50E+02	3.59E-17	2.27E-17	1.53E-17	1.21E-17	8.96E-18
3.50E+02	3.25E+02	3.50E-17	2.23E-17	1.50E-17	1.20E-17	8.84E-18
3.25E+02	3.00E+02	3.44E-17	2.21E-17	1.49E-17	1.20E-17	8.83E-18
3.00E+02	2.75E+02	3.39E-17	2.19E-17	1.49E-17	1.20E-17	8.92E-18
2.75E+02	2.50E+02	3.33E-17	2.17E-17	1.48E-17	1.20E-17	8.93E-18
2.50E+02	2.25E+02	3.25E-17	2.12E-17	1.45E-17	1.18E-17	8.76E-18
2.25E+02	2.00E+02	3.16E-17	2.07E-17	1.42E-17	1.15E-17	8.55E-18
2.00E+02	1.75E+02	3.09E-17	2.04E-17	1.40E-17	1.14E-17	8.47E-18
1.75E+02	1.50E+02	3.06E-17	2.02E-17	1.40E-17	1.14E-17	8.52E-18
1.50E+02	1.25E+02	3.06E-17	2.04E-17	1.42E-17	1.17E-17	8.72E-18
1.25E+02	1.00E+02	3.12E-17	2.09E-17	1.45E-17	1.20E-17	9.00E-18
1.00E+02	9.00E+01	3.18E-17	2.11E-17	1.46E-17	1.20E-17	9.10E-18
9.00E+01	8.00E+01	3.24E-17	2.14E-17	1.47E-17	1.20E-17	9.08E-18
8.00E+01	7.00E+01	3.34E-17	2.20E-17	1.50E-17	1.21E-17	9.10E-18
7.00E+01	6.00E+01	3.48E-17	2.29E-17	1.54E-17	1.24E-17	9.21E-18
6.00E+01	5.50E+01	3.55E-17	2.30E-17	1.54E-17	1.22E-17	9.07E-18
5.50E+01	5.00E+01	3.62E-17	2.35E-17	1.56E-17	1.23E-17	9.03E-18
5.00E+01	4.50E+01	4.12E-17	2.66E-17	1.72E-17	1.29E-17	9.08E-18
4.50E+01	4.00E+01	3.82E-17	2.47E-17	1.61E-17	1.21E-17	8.62E-18
4.00E+01	3.50E+01	3.69E-17	2.41E-17	1.58E-17	1.20E-17	8.66E-18
3.50E+01	3.00E+01	3.87E-17	2.55E-17	1.67E-17	1.28E-17	9.19E-18
3.00E+01	2.75E+01	4.09E-17	2.70E-17	1.77E-17	1.35E-17	9.74E-18
2.75E+01	2.50E+01	4.14E-17	2.75E-17	1.81E-17	1.38E-17	1.00E-17
2.50E+01	2.25E+01	4.20E-17	2.82E-17	1.88E-17	1.44E-17	1.05E-17
2.25E+01	2.00E+01	4.24E-17	2.89E-17	1.95E-17	1.51E-17	1.12E-17
2.00E+01	1.75E+01	4.28E-17	2.95E-17	2.02E-17	1.59E-17	1.20E-17
1.75E+01	1.49E+01	4.32E-17	3.05E-17	2.12E-17	1.70E-17	1.30E-17
1.49E+01	1.35E+01	3.77E-17	2.77E-17	2.03E-17	1.73E-17	1.39E-17
1.35E+01	1.22E+01	3.78E-17	2.78E-17	2.05E-17	1.76E-17	1.42E-17
1.22E+01	1.00E+01	3.77E-17	2.82E-17	2.12E-17	1.87E-17	1.55E-17
1.00E+01	8.19E+00	3.77E-17	2.85E-17	2.17E-17	1.96E-17	1.63E-17
8.19E+00	6.70E+00	4.04E-17	3.04E-17	2.36E-17	2.18E-17	1.87E-17
6.70E+00	5.49E+00	4.23E-17	3.19E-17	2.38E-17	2.13E-17	1.76E-17
5.49E+00	4.49E+00	3.89E-17	2.92E-17	2.16E-17	1.89E-17	1.54E-17
4.49E+00	3.68E+00	5.10E-17	4.12E-17	3.09E-17	2.70E-17	2.26E-17
3.68E+00	3.01E+00	5.17E-17	4.22E-17	3.21E-17	2.88E-17	2.47E-17
3.01E+00	2.47E+00	4.68E-17	3.78E-17	2.95E-17	2.72E-17	2.33E-17
2.47E+00	2.02E+00	4.91E-17	3.92E-17	3.10E-17	2.84E-17	2.45E-17
2.02E+00	1.65E+00	5.46E-17	4.44E-17	3.52E-17	3.14E-17	2.75E-17
1.65E+00	1.35E+00	5.40E-17	4.39E-17	3.50E-17	3.06E-17	2.74E-17
1.35E+00	1.11E+00	5.23E-17	4.24E-17	3.34E-17	2.88E-17	2.53E-17
1.11E+00	9.07E-01	4.86E-17	4.09E-17	3.23E-17	2.82E-17	2.53E-17
9.07E-01	7.43E-01	3.60E-17	2.85E-17	2.27E-17	2.02E-17	1.79E-17
7.43E-01	4.98E-01	2.93E-17	2.36E-17	1.89E-17	1.64E-17	1.48E-17
4.98E-01	3.34E-01	2.30E-17	2.00E-17	1.68E-17	1.42E-17	1.38E-17
3.34E-01	2.24E-01	1.59E-17	1.38E-17	1.16E-17	1.01E-17	9.77E-18
2.24E-01	1.50E-01	1.18E-17	1.03E-17	8.78E-18	7.56E-18	7.44E-18
1.50E-01	8.65E-02	8.55E-18	7.66E-18	6.70E-18	5.76E-18	5.81E-18
8.65E-02	3.18E-02	5.82E-18	5.54E-18	5.10E-18	4.39E-18	4.64E-18
3.18E-02	1.50E-02	4.44E-18	4.41E-18	4.23E-18	3.64E-18	3.97E-18
1.50E-02	7.10E-03	4.17E-18	4.21E-18	4.08E-18	3.52E-18	3.86E-18
7.10E-03	3.35E-03	4.06E-18	4.11E-18	4.01E-18	3.45E-18	3.79E-18
3.35E-03	1.58E-03	3.93E-18	3.99E-18	3.91E-18	3.37E-18	3.69E-18
1.58E-03	4.54E-04	3.76E-18	3.85E-18	3.78E-18	3.28E-18	3.58E-18
4.54E-04	1.01E-04	3.51E-18	3.60E-18	3.55E-18	3.08E-18	3.34E-18
1.01E-04	2.26E-05	3.16E-18	3.24E-18	3.17E-18	2.76E-18	2.97E-18
2.26E-05	1.07E-05	2.77E-18	2.81E-18	2.74E-18	2.36E-18	2.52E-18
1.07E-05	5.04E-06	2.53E-18	2.55E-18	2.46E-18	2.12E-18	2.24E-18
5.04E-06	2.38E-06	2.25E-18	2.25E-18	2.15E-18	1.84E-18	1.93E-18
2.38E-06	1.13E-06	1.93E-18	1.91E-18	1.80E-18	1.54E-18	1.59E-18
1.13E-06	4.14E-07	1.58E-18	1.53E-18	1.42E-18	1.21E-18	1.23E-18
4.14E-07	1.00E-10	1.02E-18	9.86E-19	9.04E-19	7.89E-19	7.67E-19

TABLE B.3

Neutron Importance vs. Energy for Specified Cosine Intervals and r = 495 m

E_{High} (MeV)	E_{Low} (MeV)	Neutron Importance [Rem (Neu.)$^{-1}$] cosθ = 0 to .2	cosθ = .2 to .4	cosθ = .4 to .6	cosθ = .6 to .8	cosθ = .8 to 1
4.00E+02	3.75E+02	6.04E-18	3.72E-18	2.39E-18	1.71E-18	9.01E-19
3.75E+02	3.50E+02	5.80E-18	3.57E-18	2.29E-18	1.63E-18	8.53E-19
3.50E+02	3.25E+02	5.62E-18	3.46E-18	2.23E-18	1.59E-18	8.28E-19
3.25E+02	3.00E+02	5.47E-18	3.37E-18	2.17E-18	1.55E-18	8.14E-19
3.00E+02	2.75E+02	5.32E-18	3.28E-18	2.12E-18	1.51E-18	7.97E-19
2.75E+02	2.50E+02	5.17E-18	3.18E-18	2.05E-18	1.46E-18	7.74E-19
2.50E+02	2.25E+02	5.00E-18	3.07E-18	1.98E-18	1.41E-18	7.46E-19
2.25E+02	2.00E+02	4.83E-18	2.95E-18	1.90E-18	1.35E-18	7.15E-19
2.00E+02	1.75E+02	4.67E-18	2.85E-18	1.83E-18	1.30E-18	6.90E-19
1.75E+02	1.50E+02	4.52E-18	2.76E-18	1.77E-18	1.25E-18	6.71E-19
1.50E+02	1.25E+02	4.39E-18	2.67E-18	1.72E-18	1.21E-18	6.53E-19
1.25E+02	1.00E+02	4.24E-18	2.58E-18	1.66E-18	1.17E-18	6.33E-19
1.00E+02	9.00E+01	4.12E-18	2.51E-18	1.61E-18	1.13E-18	6.20E-19
9.00E+01	8.00E+01	4.04E-18	2.47E-18	1.59E-18	1.12E-18	6.07E-19
8.00E+01	7.00E+01	3.94E-18	2.43E-18	1.57E-18	1.11E-18	5.96E-19
7.00E+01	6.00E+01	3.83E-18	2.39E-18	1.56E-18	1.11E-18	5.89E-19
6.00E+01	5.50E+01	3.70E-18	2.34E-18	1.52E-18	1.09E-18	5.77E-19
5.50E+01	5.00E+01	3.57E-18	2.29E-18	1.51E-18	1.09E-18	5.79E-19
5.00E+01	4.50E+01	3.37E-18	2.31E-18	1.59E-18	1.19E-18	6.54E-19
4.50E+01	4.00E+01	3.16E-18	2.13E-18	1.45E-18	1.08E-18	5.86E-19
4.00E+01	3.50E+01	2.99E-18	2.00E-18	1.36E-18	1.02E-18	5.62E-19
3.50E+01	3.00E+01	2.79E-18	1.92E-18	1.34E-18	1.03E-18	5.89E-19
3.00E+01	2.75E+01	2.57E-18	1.83E-18	1.31E-18	1.03E-18	6.12E-19
2.75E+01	2.50E+01	2.41E-18	1.75E-18	1.27E-18	1.01E-18	6.19E-19
2.50E+01	2.25E+01	2.26E-18	1.66E-18	1.22E-18	9.97E-19	6.25E-19
2.25E+01	2.00E+01	2.12E-18	1.58E-18	1.18E-18	9.77E-19	6.29E-19
2.00E+01	1.75E+01	1.97E-18	1.49E-18	1.12E-18	9.48E-19	6.28E-19
1.75E+01	1.49E+01	1.77E-18	1.35E-18	1.03E-18	8.86E-19	6.00E-19
1.49E+01	1.35E+01	1.28E-18	1.02E-18	8.24E-19	7.63E-19	5.65E-19
1.35E+01	1.22E+01	1.27E-18	1.01E-18	8.21E-19	7.64E-19	5.71E-19
1.22E+01	1.00E+01	1.29E-18	1.03E-18	8.37E-19	7.89E-19	6.00E-19
1.00E+01	8.19E+00	1.46E-18	1.13E-18	9.10E-19	8.45E-19	6.36E-19
8.19E+00	6.70E+00	1.38E-18	1.10E-18	8.98E-19	8.57E-19	6.72E-19
6.70E+00	5.49E+00	1.42E-18	1.09E-18	8.75E-19	8.10E-19	6.09E-19
5.49E+00	4.49E+00	1.28E-18	9.56E-19	7.42E-19	6.59E-19	4.78E-19
4.49E+00	3.68E+00	9.02E-19	8.00E-19	6.95E-19	6.80E-19	5.55E-19
3.68E+00	3.01E+00	9.63E-19	8.64E-19	7.61E-19	7.62E-19	6.32E-19
3.01E+00	2.47E+00	1.25E-18	1.04E-18	8.76E-19	8.41E-19	6.65E-19
2.47E+00	2.02E+00	1.27E-18	1.05E-18	8.63E-19	8.05E-19	6.27E-19
2.02E+00	1.65E+00	9.05E-19	8.09E-19	6.98E-19	6.69E-19	5.47E-19
1.65E+00	1.35E+00	6.93E-19	6.51E-19	5.79E-19	5.66E-19	4.80E-19
1.35E+00	1.11E+00	6.20E-19	5.72E-19	5.01E-19	4.80E-19	4.00E-19
1.11E+00	9.07E-01	4.14E-19	3.99E-19	3.62E-19	3.61E-19	3.16E-19
9.07E-01	7.43E-01	4.63E-19	3.98E-19	3.34E-19	3.14E-19	2.50E-19
7.43E-01	4.98E-01	2.31E-19	2.06E-19	1.76E-19	1.67E-19	1.37E-19
4.98E-01	3.34E-01	7.41E-20	7.71E-20	7.36E-20	7.11E-20	6.89E-20
3.34E-01	2.24E-01	5.95E-20	6.01E-20	5.61E-20	5.47E-20	5.07E-20
2.24E-01	1.50E-01	3.96E-20	4.11E-20	3.92E-20	3.82E-20	3.65E-20
1.50E-01	8.65E-02	2.72E-20	2.91E-20	2.84E-20	2.77E-20	2.74E-20
8.65E-02	3.18E-02	1.79E-20	1.97E-20	1.98E-20	1.89E-20	1.99E-20
3.18E-02	1.50E-02	1.13E-20	1.25E-20	1.28E-20	1.20E-20	1.31E-20
1.50E-02	7.10E-03	8.68E-21	9.62E-21	9.91E-21	9.16E-21	1.01E-20
7.10E-03	3.35E-03	6.85E-21	7.59E-21	7.83E-21	7.20E-21	8.01E-21
3.35E-03	1.58E-03	5.45E-21	6.03E-21	6.23E-21	5.71E-21	6.38E-21
1.58E-03	4.54E-04	4.37E-21	4.84E-21	5.02E-21	4.59E-21	5.15E-21
4.54E-04	1.01E-04	3.15E-21	3.48E-21	3.61E-21	3.30E-21	3.70E-21
1.01E-04	2.26E-05	2.28E-21	2.50E-21	2.60E-21	2.38E-21	2.66E-21
2.26E-05	1.07E-05	1.77E-21	1.94E-21	2.02E-21	1.86E-21	2.09E-21
1.07E-05	5.04E-06	1.62E-21	1.78E-21	1.85E-21	1.72E-21	1.93E-21
5.04E-06	2.38E-06	1.50E-21	1.65E-21	1.72E-21	1.61E-21	1.82E-21
2.38E-06	1.13E-06	1.39E-21	1.53E-21	1.61E-21	1.52E-21	1.72E-21
1.13E-06	4.14E-07	1.25E-21	1.38E-21	1.47E-21	1.41E-21	1.61E-21
4.14E-07	1.00E-10	9.83E-22	1.09E-21	1.17E-21	1.18E-21	1.36E-21

TABLE B.4

Neutron Importance vs. Energy for Specified Cosine Intervals and r = 1005 m

E_{High} (MeV)	E_{Low} (MeV)	Neutron Importance [Rem (Neu.)$^{-1}$] cosθ = 0 to .2	cosθ = .2 to .4	cosθ = .4 to .6	cosθ = .6 to .8	cosθ = .8 to 1
4.00E+02	3.75E+02	1.64E-18	1.01E-18	5.70E-19	3.11E-19	1.21E-19
3.75E+02	3.50E+02	1.58E-18	9.68E-19	5.42E-19	2.94E-19	1.14E-19
3.50E+02	3.25E+02	1.52E-18	9.27E-19	5.17E-19	2.79E-19	1.08E-19
3.25E+02	3.00E+02	1.47E-18	8.87E-19	4.92E-19	2.65E-19	1.03E-19
3.00E+02	2.75E+02	1.41E-18	8.43E-19	4.65E-19	2.49E-19	9.60E-20
2.75E+02	2.50E+02	1.35E-18	7.98E-19	4.36E-19	2.31E-19	8.87E-20
2.50E+02	2.25E+02	1.29E-18	7.55E-19	4.08E-19	2.15E-19	8.15E-20
2.25E+02	2.00E+02	1.23E-18	7.08E-19	3.79E-19	1.97E-19	7.42E-20
2.00E+02	1.75E+02	1.17E-18	6.63E-19	3.51E-19	1.81E-19	6.77E-20
1.75E+02	1.50E+02	1.10E-18	6.14E-19	3.22E-19	1.65E-19	6.13E-20
1.50E+02	1.25E+02	1.02E-18	5.60E-19	2.90E-19	1.47E-19	5.45E-20
1.25E+02	1.00E+02	9.09E-19	4.98E-19	2.58E-19	1.31E-19	4.79E-20
1.00E+02	9.00E+01	8.16E-19	4.51E-19	2.33E-19	1.17E-19	4.18E-20
9.00E+01	8.00E+01	7.51E-19	4.22E-19	2.22E-19	1.14E-19	4.06E-20
8.00E+01	7.00E+01	6.76E-19	3.91E-19	2.11E-19	1.11E-19	4.05E-20
7.00E+01	6.00E+01	5.92E-19	3.55E-19	1.98E-19	1.08E-19	4.07E-20
6.00E+01	5.50E+01	5.22E-19	3.25E-19	1.86E-19	1.04E-19	4.00E-20
5.50E+01	5.00E+01	4.64E-19	2.97E-19	1.76E-19	1.02E-19	4.19E-20
5.00E+01	4.50E+01	3.44E-19	2.56E-19	1.70E-19	1.12E-19	5.42E-20
4.50E+01	4.00E+01	3.23E-19	2.29E-19	1.47E-19	9.38E-20	4.35E-20
4.00E+01	3.50E+01	2.91E-19	2.02E-19	1.28E-19	8.08E-20	3.77E-20
3.50E+01	3.00E+01	2.31E-19	1.68E-19	1.11E-19	7.32E-20	3.69E-20
3.00E+01	2.75E+01	1.77E-19	1.36E-19	9.42E-20	6.55E-20	3.53E-20
2.75E+01	2.50E+01	1.51E-19	1.19E-19	8.39E-20	5.99E-20	3.37E-20
2.50E+01	2.25E+01	1.28E-19	1.03E-19	7.39E-20	5.42E-20	3.18E-20
2.25E+01	2.00E+01	1.09E-19	8.87E-20	6.48E-20	4.85E-20	2.94E-20
2.00E+01	1.75E+01	9.14E-20	7.51E-20	5.56E-20	4.24E-20	2.67E-20
1.75E+01	1.49E+01	7.29E-20	6.03E-20	4.52E-20	3.52E-20	2.28E-20
1.49E+01	1.35E+01	4.61E-20	3.98E-20	3.19E-20	2.73E-20	2.03E-20
1.35E+01	1.22E+01	4.48E-20	3.90E-20	3.15E-20	2.71E-20	2.03E-20
1.22E+01	1.00E+01	4.80E-20	4.08E-20	3.27E-20	2.82E-20	2.15E-20
1.00E+01	8.19E+00	6.22E-20	4.95E-20	3.79E-20	3.12E-20	2.30E-20
8.19E+00	6.70E+00	5.21E-20	4.31E-20	3.42E-20	2.96E-20	2.30E-20
6.70E+00	5.49E+00	5.31E-20	4.32E-20	3.34E-20	2.78E-20	2.05E-20
5.49E+00	4.49E+00	4.44E-20	3.48E-20	2.60E-20	2.07E-20	1.43E-20
4.49E+00	3.68E+00	1.85E-20	1.84E-20	1.66E-20	1.59E-20	1.31E-20
3.68E+00	3.01E+00	2.01E-20	1.98E-20	1.78E-20	1.71E-20	1.43E-20
3.01E+00	2.47E+00	3.22E-20	2.76E-20	2.21E-20	1.90E-20	1.45E-20
2.47E+00	2.02E+00	2.78E-20	2.34E-20	1.82E-20	1.52E-20	1.10E-20
2.02E+00	1.65E+00	1.18E-20	1.15E-20	9.94E-21	9.13E-21	7.26E-21
1.65E+00	1.35E+00	7.10E-21	7.30E-21	6.68E-21	6.45E-21	5.43E-21
1.35E+00	1.11E+00	5.71E-21	5.79E-21	5.22E-21	4.95E-21	4.08E-21
1.11E+00	9.07E-01	3.22E-21	3.35E-21	3.14E-21	3.10E-21	2.74E-21
9.07E-01	7.43E-01	4.20E-21	3.85E-21	3.20E-21	2.83E-21	2.18E-21
7.43E-01	4.98E-01	1.12E-21	1.09E-21	9.51E-22	8.77E-22	7.15E-22
4.98E-01	3.34E-01	2.27E-22	2.45E-22	2.42E-22	2.39E-22	2.37E-22
3.34E-01	2.24E-01	1.84E-22	1.97E-22	1.91E-22	1.91E-22	1.83E-22
2.24E-01	1.50E-01	1.32E-22	1.43E-22	1.41E-22	1.41E-22	1.41E-22
1.50E-01	8.65E-02	1.04E-22	1.13E-22	1.14E-22	1.14E-22	1.19E-22
8.65E-02	3.18E-02	8.64E-23	9.44E-23	9.67E-23	9.37E-23	1.03E-22
3.18E-02	1.50E-02	7.58E-23	8.30E-23	8.62E-23	8.15E-23	9.25E-23
1.50E-02	7.10E-03	7.25E-23	7.95E-23	8.30E-23	7.79E-23	8.92E-23
7.10E-03	3.35E-03	7.01E-23	7.70E-23	8.07E-23	7.55E-23	8.68E-23
3.35E-03	1.58E-03	6.80E-23	7.48E-23	7.86E-23	7.35E-23	8.47E-23
1.58E-03	4.54E-04	6.58E-23	7.25E-23	7.65E-23	7.15E-23	8.24E-23
4.54E-04	1.01E-04	6.27E-23	6.93E-23	7.32E-23	6.86E-23	7.90E-23
1.01E-04	2.26E-05	5.91E-23	6.53E-23	6.91E-23	6.51E-23	7.49E-23
2.26E-05	1.07E-05	5.50E-23	6.07E-23	6.43E-23	6.08E-23	6.99E-23
1.07E-05	5.04E-06	5.21E-23	5.75E-23	6.07E-23	5.76E-23	6.63E-23
5.04E-06	2.38E-06	4.89E-23	5.37E-23	5.66E-23	5.39E-23	6.19E-23
2.38E-06	1.13E-06	4.52E-23	4.94E-23	5.19E-23	4.96E-23	5.67E-23
1.13E-06	4.14E-07	4.11E-23	4.46E-23	4.65E-23	4.47E-23	5.06E-23
4.14E-07	1.00E-10	3.50E-23	3.76E-23	3.86E-23	3.75E-23	4.11E-23

TABLE B.5

Photon Importance vs. Energy for Specified Cosine Intervals and $\bar{r}$ = 11 m

E_{High} (MeV)	E_{Low} (MeV)	Photon Importance [Rem (Pho.)$^{-1}$] cosθ = 0 to .2	cosθ = .2 to .4	cosθ = .4 to .6	cosθ = .6 to .8	cosθ = .8 to 1
1.40E+01	1.20E+01	4.76E-19	3.48E-19	3.61E-19	2.34E-19	8.79E-20
1.20E+01	1.00E+01	4.52E-19	3.32E-19	3.40E-19	2.21E-19	8.29E-20
1.00E+01	8.00E+00	4.21E-19	3.10E-19	3.12E-19	2.03E-19	7.65E-20
8.00E+00	7.50E+00	4.00E-19	2.88E-19	3.00E-19	1.82E-19	6.47E-20
7.50E+00	7.00E+00	3.91E-19	2.83E-19	2.93E-19	1.78E-19	6.30E-20
7.00E+00	6.50E+00	3.86E-19	2.79E-19	2.87E-19	1.74E-19	6.17E-20
6.50E+00	6.00E+00	3.81E-19	2.76E-19	2.81E-19	1.71E-19	6.07E-20
6.00E+00	5.50E+00	3.77E-19	2.74E-19	2.75E-19	1.69E-19	6.02E-20
5.50E+00	5.00E+00	3.75E-19	2.82E-19	2.71E-19	1.69E-19	6.04E-20
5.00E+00	4.50E+00	3.82E-19	2.82E-19	2.65E-19	1.54E-19	6.07E-20
4.50E+00	4.00E+00	3.80E-19	2.82E-19	2.59E-19	1.54E-19	6.14E-20
4.00E+00	3.50E+00	3.80E-19	2.75E-19	2.62E-19	1.71E-19	6.53E-20
3.50E+00	3.00E+00	3.89E-19	2.96E-19	2.65E-19	1.78E-19	7.90E-20
3.00E+00	2.50E+00	4.01E-19	3.26E-19	2.78E-19	2.05E-19	1.00E-19
2.50E+00	2.00E+00	4.27E-19	3.74E-19	3.03E-19	2.54E-19	1.61E-19
2.00E+00	1.50E+00	4.91E-19	4.52E-19	3.55E-19	3.40E-19	2.92E-19
1.50E+00	1.00E+00	6.09E-19	5.73E-19	4.42E-19	4.72E-19	4.84E-19
1.00E+00	4.00E-01	7.01E-19	5.62E-19	5.18E-19	5.39E-19	5.08E-19
4.00E-01	2.00E-01	7.09E-19	5.78E-19	5.59E-19	5.84E-19	5.29E-19
2.00E-01	1.00E-01	5.86E-19	5.62E-19	4.64E-19	5.05E-19	4.14E-19
1.00E-01	1.00E-02	2.59E-19	2.65E-19	2.10E-19	3.03E-19	1.90E-19

TABLE B.6

Photon Importance vs. Energy for Specified Cosine Intervals and r = 108 m

E_{High} (MeV)	E_{Low} (MeV)	Photon Importance [Rem (Pho.)$^{-1}$] cosθ = 0 to .2	cosθ = .2 to .4	cosθ = .4 to .6	cosθ = .6 to .8	cosθ = .8 to 1
1.40E+01	1.20E+01	3.46E-19	1.42E-19	8.42E-20	6.86E-20	6.61E-20
1.20E+01	1.00E+01	3.40E-19	1.42E-19	8.32E-20	6.62E-20	6.31E-20
1.00E+01	8.00E+00	3.31E-19	1.42E-19	8.19E-20	6.32E-20	5.64E-20
8.00E+00	7.50E+00	3.49E-19	1.42E-19	7.95E-20	6.08E-20	5.75E-20
7.50E+00	7.00E+00	3.48E-19	1.42E-19	7.95E-20	6.02E-20	5.63E-20
7.00E+00	6.50E+00	3.47E-19	1.43E-19	7.97E-20	5.98E-20	5.51E-20
6.50E+00	6.00E+00	3.46E-19	1.44E-19	8.02E-20	5.95E-20	5.39E-20
6.00E+00	5.50E+00	3.44E-19	1.46E-19	8.11E-20	5.95E-20	5.21E-20
5.50E+00	5.00E+00	3.43E-19	1.48E-19	8.23E-20	5.97E-20	5.20E-20
5.00E+00	4.50E+00	3.40E-19	1.50E-19	8.36E-20	6.00E-20	5.39E-20
4.50E+00	4.00E+00	3.37E-19	1.52E-19	8.52E-20	6.04E-20	5.25E-20
4.00E+00	3.50E+00	3.32E-19	1.55E-19	8.72E-20	6.12E-20	5.12E-20
3.50E+00	3.00E+00	3.26E-19	1.58E-19	9.01E-20	6.27E-20	5.14E-20
3.00E+00	2.50E+00	3.18E-19	1.62E-19	9.40E-20	6.50E-20	5.06E-20
2.50E+00	2.00E+00	3.07E-19	1.67E-19	9.94E-20	6.88E-20	5.07E-20
2.00E+00	1.50E+00	2.92E-19	1.73E-19	1.07E-19	7.44E-20	5.18E-20
1.50E+00	1.00E+00	2.69E-19	1.79E-19	1.16E-19	8.20E-20	5.46E-20
1.00E+00	4.00E-01	2.60E-19	1.75E-19	1.16E-19	8.43E-20	6.06E-20
4.00E-01	2.00E-01	1.69E-19	1.21E-19	8.52E-20	6.43E-20	5.13E-20
2.00E-01	1.00E-01	8.83E-20	6.58E-20	4.89E-20	3.81E-20	3.28E-20
1.00E-01	1.00E-02	4.34E-21	3.28E-21	2.33E-21	1.96E-21	1.47E-21

TABLE B.7

Photon Importance vs. Energy for Specified Cosine Intervals and r = 495 m

		Photon Importance [Rem (Pho.)$^{-1}$]				
E_{High} (MeV)	E_{Low} (MeV)	cosθ = 0 to .2	cosθ = .2 to .4	cosθ = .4 to .6	cosθ = .6 to .8	cosθ = .8 to 1
1.40E+01	1.20E+01	3.45E-20	1.32E-20	4.68E-21	1.62E-21	1.77E-21
1.20E+01	1.00E+01	3.27E-20	1.27E-20	4.58E-21	1.56E-21	1.60E-21
1.00E+01	8.00E+00	3.04E-20	1.20E-20	4.49E-21	1.54E-21	1.36E-21
8.00E+00	7.50E+00	3.11E-20	1.24E-20	4.50E-21	1.42E-21	1.36E-21
7.50E+00	7.00E+00	3.02E-20	1.21E-20	4.42E-21	1.37E-21	1.29E-21
7.00E+00	6.50E+00	2.93E-20	1.18E-20	4.45E-21	1.43E-21	1.22E-21
6.50E+00	6.00E+00	2.83E-20	1.15E-20	4.55E-21	1.41E-21	1.14E-21
6.00E+00	5.50E+00	2.71E-20	1.12E-20	4.47E-21	1.51E-21	1.08E-21
5.50E+00	5.00E+00	2.58E-20	1.08E-20	4.40E-21	1.61E-21	1.03E-21
5.00E+00	4.50E+00	2.43E-20	1.03E-20	4.33E-21	1.60E-21	9.65E-22
4.50E+00	4.00E+00	2.26E-20	9.82E-21	4.23E-21	1.55E-21	9.56E-22
4.00E+00	3.50E+00	2.07E-20	9.21E-21	4.11E-21	1.78E-21	8.87E-22
3.50E+00	3.00E+00	1.85E-20	8.48E-21	3.95E-21	1.90E-21	8.21E-22
3.00E+00	2.50E+00	1.60E-20	7.61E-21	3.73E-21	1.94E-21	7.60E-22
2.50E+00	2.00E+00	1.32E-20	6.56E-21	3.43E-21	1.98E-21	8.60E-22
2.00E+00	1.50E+00	1.00E-20	5.30E-21	3.00E-21	1.93E-21	8.73E-22
1.50E+00	1.00E+00	6.64E-21	3.85E-21	2.42E-21	1.75E-21	8.67E-22
1.00E+00	4.00E-01	3.48E-21	2.33E-21	1.57E-21	1.20E-21	6.54E-22
4.00E-01	2.00E-01	7.50E-22	5.88E-22	4.45E-22	3.71E-22	2.55E-22
2.00E-01	1.00E-01	1.67E-22	1.45E-22	1.20E-22	1.08E-22	8.65E-23
1.00E-01	1.00E-02	1.32E-27	1.03E-27	6.95E-28	4.91E-28	3.79E-28

TABLE B.8

Photon Importance vs. Energy for Specified Cosine Intervals and r = 1005 m

E_{High} (MeV)	E_{Low} (MeV)	Photon Importance [Rem (Pho.)$^{-1}$] cosθ = 0 to .2	cosθ = .2 to .4	cosθ = .4 to .6	cosθ = .6 to .8	cosθ = .8 to 1
1.40E+01	1.20E+01	5.00E-21	1.70E-21	3.62E-22	3.90E-23	5.10E-24
1.20E+01	1.00E+01	4.50E-21	1.53E-21	3.58E-22	3.94E-23	4.90E-24
1.00E+01	8.00E+00	3.88E-21	1.34E-21	3.32E-22	4.70E-23	4.43E-24
8.00E+00	7.50E+00	3.68E-21	1.34E-21	3.35E-22	4.79E-23	4.40E-24
7.50E+00	7.00E+00	3.46E-21	1.26E-21	3.21E-22	4.93E-23	4.44E-24
7.00E+00	6.50E+00	3.23E-21	1.19E-21	3.09E-22	4.79E-23	4.21E-24
6.50E+00	6.00E+00	2.97E-21	1.10E-21	2.92E-22	4.63E-23	4.15E-24
6.00E+00	5.50E+00	2.70E-21	1.01E-21	2.89E-22	4.43E-23	3.78E-24
5.50E+00	5.00E+00	2.41E-21	9.13E-22	2.69E-22	4.18E-23	3.72E-24
5.00E+00	4.50E+00	2.11E-21	8.12E-22	2.50E-22	4.04E-23	3.66E-24
4.50E+00	4.00E+00	1.81E-21	7.08E-22	2.29E-22	3.92E-23	3.34E-24
4.00E+00	3.50E+00	1.50E-21	5.97E-22	2.01E-22	4.18E-23	3.10E-24
3.50E+00	3.00E+00	1.18E-21	4.83E-22	1.72E-22	4.33E-23	4.28E-24
3.00E+00	2.50E+00	8.70E-22	3.68E-22	1.40E-22	4.35E-23	5.40E-24
2.50E+00	2.00E+00	5.82E-22	2.55E-22	1.06E-22	4.04E-23	7.67E-24
2.00E+00	1.50E+00	3.33E-22	1.54E-22	7.11E-23	3.34E-23	1.12E-23
1.50E+00	1.00E+00	1.48E-22	7.41E-23	3.96E-23	2.31E-23	1.09E-23
1.00E+00	4.00E-01	3.56E-23	2.51E-23	1.65E-23	1.12E-23	5.97E-24
4.00E-01	2.00E-01	1.76E-24	1.54E-24	1.19E-24	9.54E-25	6.48E-25
2.00E-01	1.00E-01	1.68E-25	1.66E-25	1.45E-25	1.32E-25	1.08E-25
1.00E-01	1.00E-02	2.28E-36	1.57E-36	1.05E-36	6.94E-37	5.84E-37

References

1. S. J. Lindenbaum, Shielding of High-Energy Accelerators, Ann. Rev. Nucl. Sci. 11 (1961).
2. C. H. Distenfeld and R. D. Colvett, Skyshine Considerations for Accelerator Shielding Design, Nucl. Sci. Eng. 26, 117 (1966).
3. A. Rindi and R. Thomas, Skyshine - A Paper Tiger, Particle Acc. 7, 23 (1975).
4. ISABELLE, A 400x400 GeV Colliding Beam Facility, BNL-50718, Brookhaven National Laboratory (1978).
5. R. G. Alsmiller, Jr. and J. Barish, Neutron-Photon Multigroup Cross Sections for Neutron Energies $\leq$ 60 MeV, Nucl. Sci. Eng. 69, 378 (1979).
6. R. G. Alsmiller, Jr., M. Leimdorfer and J. Barish, Analytic Representation of Nonelastic Cross Sections and Particle Emission Spectra from Nucleon-Nucleus Collisions in the Energy Range 25 to 400 MeV, ORNL-4041, Oak Ridge National Laboratory (1967).
7. R. G. Alsmiller, Jr. and J. Barish, NCDATA - Nuclear Collision Data for Nucleon-Nucleus Collisions in the Energy Range 25 to 400 MeV, ORNL-4220, Oak Ridge National Laboratory (1968).
8. F. D. Bercchetti and G. N. Greenless, Nucleon-Nucleus Optical Model Parameters, A > 40, E < 50 MeV, Phys. Rev. 182, 1190 (1969).

9. R. W. Roussin, R. G. Alsmiller, Jr., J. Barish, Calculations of the Transport of Neutrons and Secondary Gamma Rays Through Concrete for Incident Neutrons in the Energy Range 15 to 75 MeV, Nucl. Eng. & Design 24, 250 (1973).

10. W. E. Ford,III et al., Modification Number One to the Coupled 100n-21γ Cross Section Library for E.P.R. Calculations, ORNL/TM-5249, Oak Ridge National Laboratory (1949).

11. Protection Against Neutron Radiation, National Council on Radiation Protection and Measurements, NCRP Report No. 38 (1971).

12. H. C. Claiborne and D. K. Trubey, Gamma Ray Dose Rates in a Slab Phantom, Nucl. Am. Tech. 8, 450 (1970).

13. W. A. Rhoades, D. B. Simpson, R. L. Childs, and W. W. Engle, Jr., The DOT-IV Two-Dimensional Discrete Ordinates Transport Code With Space-Dependent Mesh and Quadrature, ORNL/TM-6529, Oak Ridge National Laboratory (1979).

14. R. A. Lillie, R. G. Alsmiller, Jr. and J. T. Mihalczo, Design Calculations for a 14-MeV Neutron Collimator, Nucl. Tech. 43, 373 (1979).

15. F. R. Mynatt, F. J. Muckenthaler and P. N. Stevens, Development of Two-Dimensional Discrete Ordinates Transport Theory for Radiation Shielding, Union Carbide Corporation, Nuclear Division, Computing Technology Center, CTC-INF-952 (1969).

16. D. E. Bartine et al., Low-Energy Electron Transport by the Method of Discrete Ordinates, Nucl. Sci. Eng. 48, 159 (1972).

17. R. Madey, A. R. Baldwin and F. M. Waterman, Neutron Spectrum from 20 to About 600 MeV Above the Brookhaven National Laboratory AGS Shielding, Trans. Am. Nucl. Soc. 23, 612 (1976).

18. T. W. Armstrong, K. C. Chandler and J. Barish, Calculations of Neutron Flux Spectra Indicued in the Earth's Atmosphere by Galactic Cosmic Rays, J. Geop. Res. 78, 2715 (1973).

19. K. C. Chandler and T. W. Armstrong, Operating Instructions for the High-Energy Nucleon-Meson Transport Code HETC, Oak Ridge National Laboratory, ORNL-4744 (1972).

20. M. B. Emmett, The MORSE Monte Carlo Radiation Transport System, Oak Ridge National Laboratory, ORNL-4972 (1975).

21. T. W. Armstrong et al., Monte Carlo Calculations of High-Energy Nucleon-Meson Cascades and Comparison With Experiment, Nucl. Sci. Eng. 49, 89 (1972).

22. A. Van Ginneken, CASIM, A Program to Simulate Transport of Hadronic Cascades in Matter, Fermi National Laboratory, FNL-272 (1975).

ORNL/TM-7512
Dist. Category UC-20d

Internal Distribution

1-2. L. S. Abbott
3. F. S. Alsmiller
4-13. R. G. Alsmiller, Jr.
14-17. J. Barish
18. J. M. Barnes
19. D. E. Bartine
20. L. A. Berry
21. B. L. Bishop
22. A. A. Brooks
23-27. R. L. Childs
28. EPIC
29. G. F. Flanagan
30. T. A. Gabriel
31. H. Goldstein (Consultant)
32. R. A. Lillie
33-42. F. C. Maienschein
43. J. V. Pace, III
44. R. W. Peelle
45. R. W. Roussin
46. R. T. Santoro
47. C. R. Weisbin
48. G. E. Whitesides
49. A. Zucker
50. P. Greebler (Consultant)
51. H. J. C. Kouts (Consultant)
52. W. B. Loewenstein (Consultant)
53. R. Wilson (Consultant)
54-55. Central Research Library
56. ORNL Y-12 Technical Library - Document Reference Section
57-58. Laboratory Records
59. ORNL Patent Office
60. Laboratory Records - RC
61-66. EPD Reports Office

External Distribution

67. Office of Assistant Manager, Energy Research and Development, DOE-ORO, Oak Ridge, TN 37830
68. R. Fricken, Office of Basic Energy Sciences, Department of Energy, Washington, DC 20545
69. P. Gollon, Brookhaven National Laboratory, Associated Universities, Inc., Upton, NY 11973
70. A. Stevens, Brookhaven National Laboratory, Associated Universities, Inc., Upton, NY 11973
71. W. A. Wallenmeyer, Office of Basic Energy Sciences, Department of Energy, Washington, DC 20545
72-119. Given High-Energy Accelerator Shielding distribution.
120-257. Given distribution as shown in TID-4500, Magnetic Fusion Energy (Distribution Category UC-20d: Fusion Systems)